Journal of Asian Earth Sciences 53 (2012) 67–81

Contents lists available at SciVerse ScienceDirect

Journal of Asian Earth Sciences

journal homepage: www.elsevier.com/locate/jseaes

Late Cretaceous (ca. 90 Ma) adakitic intrusive rocks in the Kelu area, Gangdese Belt (southern Tibet): Slab melting and implications for Cu–Au mineralization

Zi-Qi Jiang [a,b,c], Qiang Wang [a,*], Zheng-Xiang Li [d], Derek A. Wyman [e], Gong-Jian Tang [a,b], Xiao-Hui Jia [a,b], Yue-Heng Yang [f]

[a] State Key Laboratory of Isotope Geochemistry, Guangzhou Institute of Geochemistry, Chinese Academy of Sciences, Guangzhou 510640, PR China
[b] Graduate University of Chinese Academy of Sciences, Beijing 100049, PR China
[c] Key Laboratory of Marginal Sea Geology, South China Sea Institute of Oceanology, Chinese Academy of Sciences, Guangzhou 510301, PR China
[d] ARC Centre of Excellence for Core to Crust Fluid Systems (CCFS) and The Institute for Geoscience Research (TIGeR), Department of Applied Geology, Curtin University, Perth, WA 6845, Australia
[e] School of Geosciences, The University of Sydney, NSW 2006, Australia
[f] Institute of Geology and Geophysics, Chinese Academy of Sciences, Beijng 100029, PR China

ARTICLE INFO

Article history:
Received 14 January 2011
Received in revised form 7 February 2012
Accepted 19 February 2012
Available online 23 March 2012

Keywords:
Adakite
Cu–Au mineralization
Slab melting
Gangdese arc
Tibet

ABSTRACT

The Gangdese Belt in southern Tibet (GBST) is a major Cu–Au–Mo mineralization zone that mostly formed after the India–Asia collision in association with the small-volume, though widespread, Miocene (18–10 Ma) adakitic porphyries. Cu–Au mineralization has scarcely been found in the regional Jurassic–Early Tertiary batholiths related to subduction of the Neo-Tethyan oceanic plate. Here, we report petrological, zircon geochronological and geochemical data for Late Cretaceous (~90 Ma) intrusive rocks that contain Cu–Au mineralization from the Kelu area in the GBST. These rocks consist of quartz monzonites and diorites. The quartz monzonites, with SiO_2 of 58–59 wt.% and Na_2O/K_2O of 1.1–1.2, are geochemically similar to slab-derived adakites characterized by apparent depletions in heavy rare earth elements (e.g., Yb = 1.4–1.5 ppm) and Y (16–18 ppm) contents, positive Sr but negative Nb and Ti anomalies on multi-element variation diagrams. They have relatively low $(^{87}Sr/^{86}Sr)_i$ (0.7038–0.7039) ratios and high $\varepsilon_{Nd}(t)$ (+3.4 to +3.9) and in situ zircon $\varepsilon_{Hf}(t)$ (+9.3 to +15.8) values. The diorites exhibit high Mg-numbers (0.57–0.61) similar to those of magnesian andesites, and have $(^{87}Sr/^{86}Sr)_i$ (0.7040–0.7041) and $\varepsilon_{Nd}(t)$ (+3.0 to +4.4) values similar to those of the quartz monzonites. We suggest that the quartz monzonitic magmas were most likely generated by partial melting of the subducted Neo-Tethyan basaltic oceanic crust and minor associated oceanic sediments, with subsequent melt–mantle interaction, and the dioritic magmas were mainly derived by the interaction between slab melts and mantle wedge peridotites, with fractionation of apatite and hornblende. These slab-derived adakitic magmas have high oxygen fugacity that may have facilitated Cu–Au mineralization. The close association of the Late Cretaceous adakitic intrusive rocks and Cu–Au mineralization in the Kelu area suggests that the arc magmatic rocks in the GBST may have higher potential than previously thought for Cu–Au mineralization.

1. Introduction

Subduction zones have been considered as a uniquely favorable tectonic setting for the generation of Cu–Au deposits (Oyarzun et al., 2001; Defant et al., 2002; Mungall, 2002; Reich et al., 2003; Cooke et al., 2005; Sun et al., 2010). Most known porphyry/hydrothermal Cu–Au deposits in the world occur in subduction zones or arc settings (Sajona et al., 1993; Skewes and Stern, 1994; Akira, 2002; González-Partida et al., 2003; Reich et al., 2003; Cooke et al., 2005; Richards and Kerrich, 2007; Sun et al., 2010; Tang et al., 2010). These include super-giant porphyry Cu–Au deposits such as the E1 Teniente, Chuquicamata and Río Blanco–Los Bronces deposits in the Andes arc related to the subduction of oceanic crust or ridges (Skewes and Stern, 1994; Oyarzun et al., 2001; Reich et al., 2003; Cooke et al., 2005).

The Gangdese Belt in southern Tibet (GBST) contains large scale Jurassic–Early Tertiary arc calc-alkaline magmatic rocks related to the northward subduction of the Neo-Tethyan Ocean (Chung et al., 2005; Wen et al., 2008b; Ji et al., 2009a), as well as some potassic or ultra-potassic and adakitic magmatic rocks generated during continental convergence after the initial India–Asia collision (Fig. 1a) (Chung et al., 1998, 2003; Hou et al., 2004; Nomade et al., 2004; Qu et al., 2004; Williams et al., 2004; Gao et al., 2007, 2010a; Guo et al., 2007b; Xu et al., 2009; Zhao et al., 2009). In recent decades, mineral exploration in the GBST has discovered numerous

* Corresponding author.
E-mail address: wqiang@gig.ac.cn (Q. Wang).

1367-9120/$ - see front matter © 2012 Elsevier Ltd. All rights reserved.
http://dx.doi.org/10.1016/j.jseaes.2012.02.010

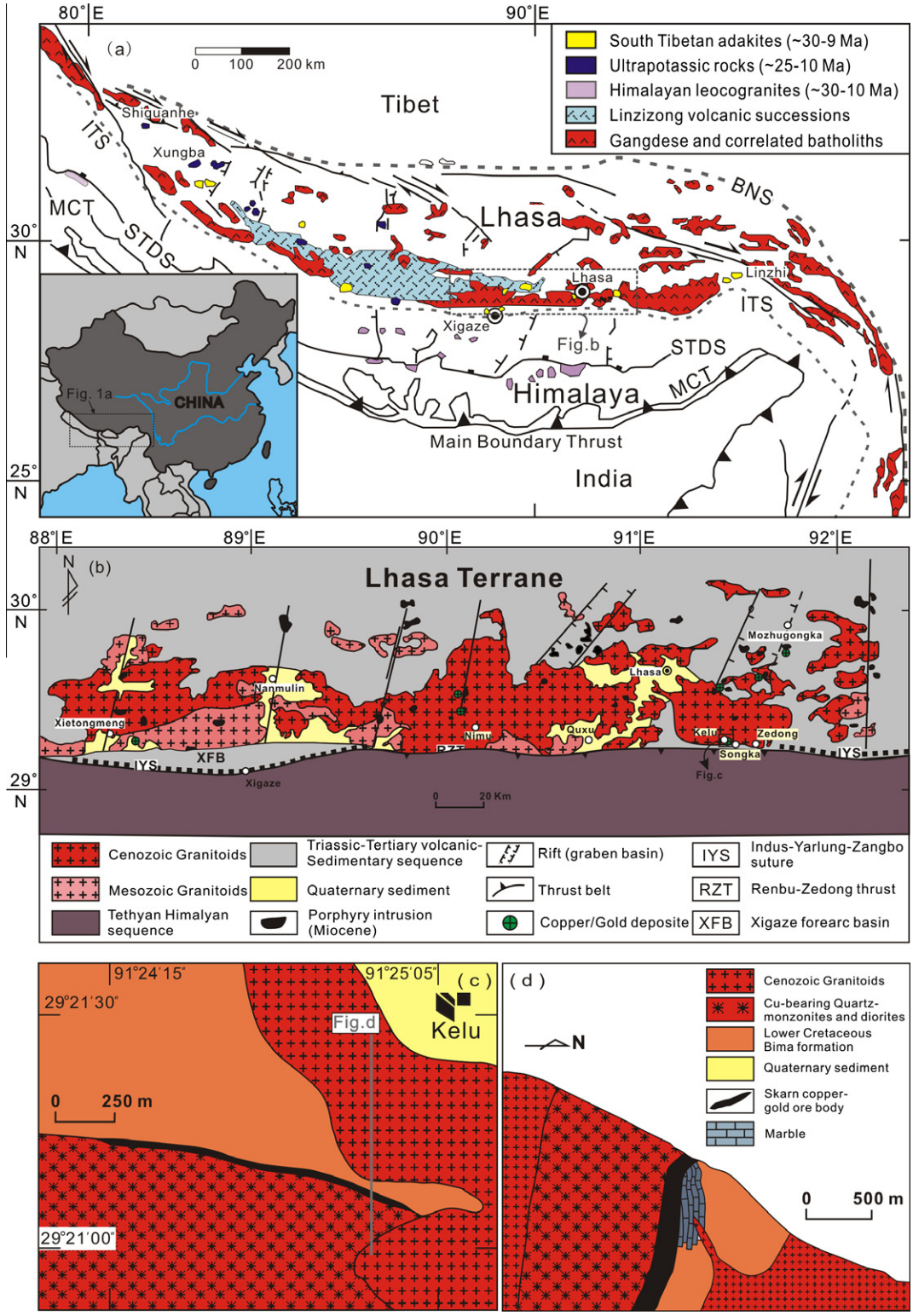

Fig. 1. (a) Simplified geological map of the Tibetan Plateau and magmatic rocks in the Lhasa Block of southern Tibet (modified from Chung et al., 2009). (b) Simplified tectonic map and location of ore-bearing adakitic intrusions of the Gangdese Belt in southern Tibet (modified from Hou et al., 2004). (c) Simplified geological map of the Kelu area in southern Gangdese Belt and (d) cross section of the Kelu Cu–Au ore deposit (modified from Li et al., 2006a,b).

Cu–Au–Mo deposits (Fig. 1b) (Qu et al., 2004; Hou et al., 2004, 2009; Hou and Cook, 2009). So far, almost all reported Cu–Au–Mo deposits in this belt were formed during continental convergence after the initial India–Asia collision, and were mainly associated with Miocene (18–10 Ma) adakitic porphyries (Hou et al., 2004, 2009; Gao et al., 2007; Guo et al., 2007b; Qu et al., 2007) and, except for one porphyry copper–gold deposit associated with a Jurassic (~172 Ma) intrusion (Tafti et al., 2009), few occurrences were found to be associated with the Cretaceous arc magmatic rocks.

This study focuses on intrusive rocks closely associated with Cu–Au deposits in the Kelu area of the GBST, and includes detailed petrological, geochronological and geochemical analyses. Our

results show that the intrusive rocks were generated in the Late Cretaceous and are geochemically similar to slab-derived adakites, thus pointing out the potential for discovering more Cu–Au deposits related to Cretaceous arc magmatism in the GBST.

2. Geological background and sample description

The Tibetan Plateau comprises, from north to south, the Songpan-Ganzi, Qiangtang, Lhasa and Himalaya Blocks (Yin and Harrison, 2000; Chung et al., 2005), which are separated by the Jinshajiang, Bangong–Nujiang and Yarlung–Tsangpo sutures, respectively. The Lhasa Block is bounded by the Bangong–Nujiang suture to the north and Yarlung–Tsangpo suture to the south (Fig. 1a) (Yin and Harrison, 2000). The Yarlung–Tsangpo suture marks the final collision between India and Asia in the Early Tertiary (~65–55 Ma) (Patzelt et al., 1996; Ding et al., 2005; Najman, 2006; Mo et al., 2007; Wu et al., 2007; Chung et al., 2009; Chen et al., 2010). A remarkable tectonic feature in the southern Lhasa Block is the occurrence of the NS-striking normal faulting or graben systems, possibly due to east–west extension during the Miocene (18–13 Ma) (Williams et al., 2001; Nomade et al., 2004) (Fig. 1b). Mesozoic–Cenozoic magmatic rocks are widespread along the southern margin of the Lhasa Block and form the well-known Gangdese magmatic belt (Fig. 1a).

The Gangdese magmatic belt contains the Gangdese batholith and Linzizong volcanic rocks. They were mainly generated between the Late Jurassic and the Early Tertiary as the result of the northward subduction, or possibly the breakoff of the Neo-Tethyan oceanic crust beneath the Lhasa Block (Zhou et al., 2004; Chung et al., 2005; Mo et al., 2008; Wen et al., 2008b; Ji et al., 2009a; Lee et al., 2009), and are considered to be an Andean-type arc magmatic belt (Wen et al., 2008b; Ji et al., 2009a). A period of magmatic quiescence between 40 and 25 Ma in the GBST (Chung et al., 2005) was followed in the Oligocene–Miocene (~26–8 Ma) by potassic or ultra-potassic volcanism (Turner et al., 1996; Miller et al., 1999; Ding et al., 2003; Gao et al., 2009; Zhao et al., 2009) and potassium-rich adakitic porphyries (Chung et al., 2003; Hou et al., 2004; Qu et al., 2004; Gao et al., 2007, 2010b; Guo et al., 2007b; Xu et al., 2009). Adakitic porphyries associated with Cu–Au–Mo mineralization were mainly formed during ~18–13 Ma (Hou et al., 2004, 2009; Wang et al., 2010a).

The Kelu area is located in the southern part of the Gangdese Belt just north of the Yarlung–Tsangpo suture, and is dominated by Late Cretaceous–Early Tertiary granitoids (Fig. 1b and c). The strata in this area consist of Cretaceous–Tertiary volcanic sedimentary sequences, e.g., the Lower Cretaceous Bima Formation, consisting of tuffaceous andesites and quartz sandstones. The Kelu skarn Cu–Au ore deposit is located about 6 km north of the Yarlung–Tsangpo River, and contains ~15.5 Mt Cu with grades of 0.11–13.09% Cu (up to 26.37%) and some Au (with grades up to 0.02%) (Zhang, 2005; Li et al., 2006a,b). A cross section based on drill hole data (Fig. 1d) illustrates that the thickness and grade of the ore body increases with depth. This indicates that the erosion depth in the ore district is shallow and that there is great potential of additional resources at depth and laterally (e.g., Li et al., 2006a,b). The Cu–Au mineralization is mainly associated with quartz monzonites and diorites, but not with adjacent granitoid intrusions (Fig. 1c). The Kelu quartz monzonites have fine- to medium-grained texture, consisting of K-feldspar (40–45 vol.%), plagioclase (35–40 vol.%), hornblende (15–20 vol.%), anhedral quartz (~5 vol.%), biotite (~5 vol.%) and minor accessory minerals (zircon, apatite and magnetite). The diorites are mainly composed of subhedral amphibole (45–50 vol.%), plagioclase (25–30 vol.%), K-feldspar (20–25 vol.%), and minor euhedral to rounded zircon, prismatic to acicular apatite and magnetite.

3. Analytical procedures

To determine the emplacement ages of intrusive rocks that are directly associated with Cu–Au mineralization in the Kelu area, three samples were chosen for LA-ICPMS zircon U–Pb dating. Zircon grains were separated from two quartz monzonite samples (07TB33b-2 and 0733a-1) and a diorite sample (07TB33d) using conventional heavy liquid and magnetic separation techniques and then purified by handpicking under a binocular microscope. Zircons >30 μm were selected and mounted in epoxy resin. The mounts were then polished and zircons photographed under a microscope. Cathodoluminescence (CL) images were taken on a JEOL JXA-8100 Superprobe Micro-analyzer with a Mono CL3 Cathodoluminescence system for high resolution imaging and spectroscopy at the State Key Laboratory of Isotope geochemistry (SKLIG), Guangzhou Institute of Geochemistry, Chinese Academy of Sciences (GIG–CAS), in order to characterize the internal structures and choose potential target sites for U–Pb dating.

Zircon U–Pb isotope compositions of sample 07TB33b-2 were analyzed with an Agilent 7500a Q-ICPMS connected to a 193 nm excimer laser ablation system at the Institute of Geology and Geophysics, Chinese Academy of Sciences, Beijing (IGG–CAS). Helium carrier gas transported the ablated sample materials from the laser-ablation cell via a mixing chamber to the ICPMS after mixing with Ar gas. Every 5 sample analyses were followed by one standard zircon 91500 (Wiedenbeck et al., 1995) and one NIST SRM 610 measurement. Details of the analytical techniques are described in Xie et al. (2008). Data reduction and fractionation correction for U–Pb analyses were done using GLITTER 4.0 (Jackson et al., 2004). Common Pb was corrected by ComPbCorr#3 17 (Andersen, 2002) for those with common $^{206}Pb > 1\%$. The U–Pb ages were calculated using the U decay constants recommended by Steiger and Jäger (1977) and Isoplot/Ex_ver3 (Ludwig, 2003). The zircon U–Pb age results are listed in Table 1.

Zircon U–Pb dating of samples 07TB33a-1 and 07TB33d were determined with an Agilent 7500a ICP-MS coupled to a Resonetic RESOLution M-50(193 nm ArF-Excimer) laser system at the SKLIG, GIG-CAS. Detailed descriptions of the instrumentation and analytical procedure were given by Tu et al. (2011). Sample mounts were placed in a specially designed double volume sample cell flushed with Ar and He. Laser energy was 80 mJ and frequency was 10 Hz with an ablation spot size of 31 μm in diameter and 40 s ablation time. The ablated material was carried by the He–Ar gas via a custom-made Squid system to homogenize signal to the ICP–MS. NIST 610 and TEM were used as external calibration standards and ^{95}Zr as the internal standard. The time-resolved spectra were processed off-line using the ICPMSDataCal software (Liu et al., 2010a,b). Common Pb correction and ages of the samples were calculated by ComPbCorr#3_17 (Andersen, 2002). Concordia diagrams and weighted mean calculations were made using Isoplot/Ex_ver3 (Ludwig, 2003). The zircon U–Pb age results are listed in Table 1.

Rock samples were examined under optical microscopy, and unaltered or least-altered samples were selected for geochemical analyses. All samples were crushed into small chips after removal of weathered rims. Fresh chips were selected and washed using distilled water in an ultrasonic bath. The chips were then powdered to 200 mesh in a Tungsten carbide mill to avoid contamination. Loss on ignition (LOI) was determined at 980 °C for 90 min. The major element composition was measured by a Rigaku RIX 2000 X-ray fluorescence spectrometer at the SKLIG, GIG–CAS, following the procedures described by Li et al. (2006a,b), and analytical uncertainties are less than 2%. Trace elements were analyzed using a Perkin–Elmer Sciex ELAN 6000 ICP–MS at the GIG–CAS. Detailed analysis or analytical procedures are described by Li et al.

Table 1
Zircon age data acquired by LA-ICPMS methods for the Kelu intrusive rocks in southern Tibet.

Analysis	Th (ppm)	U (ppm)	Th/U	Raw ratios								Apparent ages (Ma)			
				$^{207}Pb/^{206}Pb$	1σ	$^{207}Pb/^{235}U$	1σ	$^{206}Pb/^{238}U$	1σ	$^{206}Pb/^{238}U$	1σ	$^{207}Pb/^{235}U$	1σ	$^{207}Pb/^{206}Pb$	1σ
07TB33a-1															
1	202	227	0.89	0.05730	0.00788	0.10107	0.01339	0.01406	0.00092	90	6	98	12	503	180
2	275	269	1.02	0.05102	0.00493	0.09779	0.00891	0.01410	0.00049	90	3	95	8	242	143
3	211	312	0.68	0.05329	0.00885	0.09868	0.01564	0.01454	0.00076	93	5	96	14	341	261
4	958	702	1.36	0.05209	0.00400	0.09702	0.00691	0.01453	0.00050	93	3	94	6	289	101
5	524	505	1.04	0.04861	0.00547	0.09137	0.01013	0.01387	0.00039	89	3	89	9	129	195
6	306	329	0.93	0.04383	0.00792	0.09123	0.01820	0.01427	0.00073	91	5	89	17	79	254
7	1210	786	1.54	0.04818	0.00353	0.09454	0.00721	0.01416	0.00034	91	2	92	7	108	125
8	923	615	1.50	0.05464	0.00688	0.10848	0.01416	0.01433	0.00059	92	4	105	13	397	217
9	339	341	0.99	0.05882	0.00595	0.11169	0.00960	0.01433	0.00048	92	3	108	9	561	130
10	315	433	0.73	0.05111	0.00549	0.10027	0.00946	0.01471	0.00049	94	3	97	9	246	153
11	203	175	1.16	0.06189	0.00792	0.11634	0.01320	0.01427	0.00084	91	5	112	12	670	145
12	2785	1468	1.90	0.04793	0.00218	0.09283	0.00419	0.01401	0.00029	90	2	90	4	96	65
13	469	531	0.88	0.04790	0.00501	0.09101	0.00856	0.01384	0.00044	89	3	88	8	94	150
14	247	248	1.00	0.05224	0.00783	0.09888	0.01380	0.01407	0.00045	90	3	96	13	296	256
15	2496	1273	1.96	0.04913	0.00284	0.09864	0.00557	0.01453	0.00027	93	2	96	5	154	95
16	355	507	0.70	0.04789	0.00372	0.09311	0.00761	0.01408	0.00040	90	3	90	7	94	128
17	1566	888	1.76	0.04839	0.00508	0.09571	0.00993	0.01455	0.00046	93	3	93	9	118	172
18	438	344	1.27	0.05932	0.00669	0.10490	0.01111	0.01378	0.00054	88	3	101	10	579	163
19	1016	536	1.90	0.04883	0.00410	0.09403	0.00746	0.01434	0.00040	92	3	91	7	140	126
20	374	319	1.17	0.05982	0.00662	0.11220	0.01121	0.01445	0.00052	92	3	108	10	597	154
21	360	333	1.08	0.04932	0.00627	0.09603	0.01226	0.01386	0.00052	89	3	93	11	163	217
22	437	339	1.29	0.05058	0.00871	0.09596	0.01491	0.01443	0.00072	92	5	93	14	222	254
23	2100	2176	0.96	0.04847	0.00212	0.09870	0.00445	0.01450	0.00028	93	2	96	4	122	69
24	147	226	0.65	0.05634	0.01236	0.10828	0.02335	0.01394	0.00056	89	4	104	21	466	439
25	187	212	0.88	0.06430	0.00943	0.12237	0.01768	0.01435	0.00067	92	4	117	16	752	230
26	406	331	1.23	0.05870	0.00545	0.11291	0.01038	0.01425	0.00041	91	3	109	9	556	151
27	424	430	0.99	0.05058	0.00498	0.09776	0.00819	0.01464	0.00042	94	3	95	8	222	138
28	95.3	173	0.55	0.06120	0.00836	0.11770	0.01393	0.01447	0.00065	93	4	113	13	646	179
29	89.7	200	0.45	0.05862	0.00908	0.11409	0.01766	0.01396	0.00059	89	4	110	16	553	268
07TB33b-2															
1	695	516	1.35	0.05732	0.00871	0.11575	0.01699	0.01469	0.00061	94	4	111	15	504	252
2	658	453	1.45	0.05696	0.00991	0.11508	0.01920	0.01469	0.00075	94	5	111	17	490	281
3	700	528	1.33	0.07095	0.00792	0.14358	0.01514	0.01471	0.00057	94	4	136	13	956	153
4	768	494	1.55	0.05282	0.00908	0.10687	0.01760	0.01470	0.00075	94	5	103	16	321	273
5	542	469	1.16	0.04605	0.01250	0.08734	0.02330	0.01376	0.00069	88	4	85	22		443
6	581	417	1.39	0.05611	0.01049	0.11288	0.02021	0.01460	0.00082	93	5	109	18	457	299
7	785	512	1.53	0.04445	0.00693	0.09014	0.01380	0.01470	0.00048	94	3	88	13	47	220
8	938	548	1.71	0.06831	0.00719	0.13730	0.01379	0.01456	0.00049	93	3	131	12	878	153
9	1794	997	1.80	0.05018	0.00619	0.10184	0.01223	0.01471	0.00045	94	3	98	11	203	213
10	342	289	1.19	0.05234	0.02460	0.10675	0.04909	0.01478	0.00147	95	9	103	45	300	665
11	308	269	1.14	0.04804	0.02098	0.09743	0.04154	0.01469	0.00142	94	9	94	38	101	571
12	359	311	1.15	0.04990	0.01258	0.10042	0.02484	0.01459	0.00072	93	5	97	23	191	445
13	590	461	1.28	0.04605	0.02095	0.08599	0.03842	0.01354	0.00116	87	7	84	36		763
14	1194	746	1.60	0.04638	0.00400	0.09399	0.00781	0.01469	0.00038	94	2	91	7	17	133
07TB33d															
1	239	241	0.99	0.05636	0.01184	0.10822	0.02244	0.01393	0.00048	89	3	104	21	467	434
2	84.6	92.3	0.92	0.06390	0.01416	0.12727	0.02735	0.01424	0.00100	91	6	122	25	738	347
3	355	281	1.26	0.06085	0.00685	0.11390	0.01428	0.01394	0.00058	89	4	110	13	634	201
4	183	214	0.85	0.07082	0.00694	0.13448	0.01250	0.01434	0.00050	92	3	128	11	952	134
5	462	454	1.02	0.04885	0.00360	0.09088	0.00660	0.01396	0.00046	89	3	88	6	140	104
6	154	193	0.80	0.06196	0.00525	0.12172	0.01146	0.01436	0.00052	92	3	117	10	673	140
7	119	179	0.66	0.06034	0.00616	0.11413	0.01053	0.01430	0.00053	92	3	110	10	616	136

8	214	228	0.94	0.05265	0.00775	0.10031	0.01411	0.01419	0.00063	91	4	97	13	314	235		
9	115	144	0.80	0.07576	0.01594	0.12201	0.01404	0.01399	0.00065	90	4	117	13	1089	157		
10	124	135	0.92	0.06128	0.01267	0.10141	0.01772	0.01428	0.00107	91	7	98	16	649	252		
11	136	155	0.88	0.06601	0.00707	0.12030	0.01025	0.01418	0.00062	91	4	115	9	807	107		
12	289	285	1.01	0.04892	0.00893	0.09584	0.01562	0.01420	0.00077	91	5	93	14	144	250		
13	1941	798	2.43	0.04809	0.00268	0.09320	0.00509	0.01410	0.00031	90	2	90	5	104	83		
14	282	300	0.94	0.05059	0.00792	0.09301	0.01261	0.01408	0.00063	90	4	90	12	222	222		
15	109	106	1.03	0.05809	0.00859	0.11037	0.01456	0.01382	0.00072	88	5	106	13	533	200		
16	187	209	0.90	0.06418	0.00937	0.11531	0.01485	0.01409	0.00062	90	4	111	14	747	200		
17	275	284	0.97	0.05918	0.00914	0.11045	0.01435	0.01448	0.00072	93	5	106	13	574	199		
18	230	243	0.94	0.06279	0.00763	0.11097	0.01207	0.01370	0.00046	88	3	107	11	701	176		

(2006a,b), and analytical precision for most elements is better than 3%. The major and trace element results are listed in Table 2.

Whole-rock Nd and Sr isotopic compositions were determined using a Micromass Isoprobe multi-collector ICPMS at the SKLIG, GIG–CAS, following analytical procedures similar to that described by Li et al. (2004) and Wei et al. (2002). Sr and REE were separated using cation columns, and Nd fractions were further separated by HDEHP-coated Kef columns. The reported $^{87}Sr/^{86}Sr$ and $^{143}Nd/^{144}Nd$ ratios were adjusted to the NBS SRM 987 standard $^{87}Sr/^{86}Sr = 0.710243 \pm 14$ ($2\sigma m$) and the Shin Etsu JNdi-1 standard $^{143}Nd/^{144}Nd = 0.512124 \pm 11$ ($2\sigma m$). The measured Nd and Sr isotope ratios were normalized to $^{146}Nd/^{144}Nd = 0.7219$ and $^{86}Sr/^{88}Sr = 0.1194$, respectively. The Nd–Sr isotope results are listed in Table 3.

In situ zircon Hf isotopic composition analyses were obtained using a Neptune MC–ICP–MS, equipped with a 193-nm laser at the IGG–CAS. A spot size of 32 μm was used for analysis, with a laser repetition rate of 10 Hz at 100 mJ. The detailed analytical methods are described in Wu et al. (2006). During the analytical period, the $^{176}Hf/^{177}Hf$ and $^{176}Lu/^{177}Hf$ ratios of the standard zircon (91500) were 0.282294 ± 15 ($2\sigma_n$, $n = 20$) and 0.00031, similar to the low peaks of $^{176}Hf/^{177}Hf$ ratios of 0.282284 ± 22 measured by Griffin et al. (2006). The zircon Hf isotope results are listed in Table 4.

4. Results

4.1. Zircon U–Pb geochronology

The zircons of three samples (07TB33b-2, 07TB33a-1 and 07TB33d) have size ranges of 40–200 μm and length/width ratios of 1:1–3:1, and are mostly euhedral to subhedral and prismatic. CL images of zircon grains used for LA–ICP–MS analysis show no inherited cores (Fig. 2), and exhibit high Th/U ratios (0.45–1.96 for the quartz monzonite samples (07TB33b-2 and 07TB33a-1) and 0.66–2.43 for the diorite sample (07TB33d), respectively), suggesting a magmatic origin (Belousova et al., 2002). Concordia diagrams and representative CL images of analyzed zircons are shown in Fig.2.

Twenty-nine zircon analyses from the quartz monzonite sample (07TB33a-1), give a weighted mean $^{206}Pb/^{238}U$ age of 91.3 ± 1.6 Ma (2σ) (mean square weighted deviation (MSWD) = 0.32) (Fig. 2a). Fourteen analyses of zircons from the other quartz monzonite sample (07TB33b-2) yielded a weighted mean $^{206}Pb/^{238}U$ age of 93.3 ± 2.0 Ma (MSWD = 0.23) (2σ) (Fig. 2b). Thus, the age data of both samples suggest that the Kelu quartz monzonites were generated in the Late Cretaceous (~91–93 Ma). In addition, eighteen analyses of zircons from the diorite sample (07TB33d) resulted in a weighted mean $^{206}Pb/^{238}U$ age of 90.3 ± 2.1 Ma (MSWD = 0.16) (2σ) (Fig. 2c). This age is interpreted to be the best estimate of the crystallization age of the diorites. Therefore, the quartz monzonites and diorites in the Kelu Cu–Au mineralization area were formed approximately synchronously in the Late Cretaceous (~90 Ma).

4.1.1. Major and trace elements

Samples of the Kelu intrusive rocks mainly plot in the sub-alkaline field on the total alkalis-silica diagram (Fig. 3a). The diorites and quartz monzonites have SiO_2 contents of 52.17–52.86 wt.% and 57.69–59.26 wt.%, respectively. The diorite samples plot in the field of medium- and high-K calc-alkaline magmatic rocks, and the quartz monzonite samples all plot in the field of high-K calc-alkaline magmatic rocks (Fig. 3b). However, all samples exhibit high Na_2O ($Na_2O/K_2O = 1.08–6.51$) and metaluminous characteristics (A/CNK (Molar $Al_2O_3/(K_2O + Na_2O + CaO)$) = 0.73–0.88) (Table 2).

The Quartz monzonite samples show negligible Eu anomalies, but the diorite samples exhibit slightly positive Eu anomalies (Fig. 4a). However, all samples exhibit enrichments in light rare earth elements (REEs), positive Sr anomalies and depletions in heavy REEs, Nb, Ta and Ti (Fig. 4b). Moreover, they have high Sr (656–937 ppm) contents, Sr/Y (40–70) ratios and low Y (10.5–17.5 ppm) and Yb (1.06–1.53 ppm) contents, similar to those of adakites defined by Defant and Drummond (1990) (Fig. 3c), with the exception of the diorite samples that have relatively low SiO_2 contents (<56 wt.%). The diorite samples have high MgO contents (5.54–5.57 wt.%) and $Mg^{\#}$ (0.57–0.61) relative to the quartz monzonite samples (3.12–3.55 wt.% and 0.47–0.52), and are similar to those of magnesian andesites (Escuder et al., 2007; Wang et al., 2008a; Manikyamba et al., 2009). However, they have slightly higher V (165–220 ppm), more variable Cr (18.0–86.0 ppm) and Ni (11.0–48.0 ppm) and lower Zr/Sm (14–18) than the quartz monzonite samples, which have ranges between (136–144 ppm), (43.0–55.0 ppm), (27.0–41.0 ppm) and (18–32) respectively (Table 2).

4.2. Sr–Nd–Hf isotope compositions

The Kelu quartz monzonites have relatively homogeneous ($^{87}Sr/^{86}Sr)_i$ ratios (0.7038–0.7039), $\varepsilon_{Nd}(t)$ values (+3.4 to +3.9) and Nd model ages (519–557 Ma). The Kelu diorites have homogeneous ($^{87}Sr/^{86}Sr)_i$ ratios (0.7040–0.7041) and slightly variable $\varepsilon_{Nd}(t)$ values (+3.0 to +4.4) (Table 3) (Fig. 5a). Zircons from the quartz monzonite sample (07TB33b-2) have slightly variable in situ $^{176}Hf/^{177}Hf$ (0.282978–0.283162) and $\varepsilon_{Hf}(t)$ values (+9.3 to

Table 2
Major oxides (wt.%) and trace element (ppm) compositions of the Kelu intrusive rocks in southern Tibet.

Rock-type	Q-monzonite				Diorite		
Sample no.	07TB33a-1	07TB33b-1	07TB33b-2	07TB33e	07TB33a-2	07TB33c-1	07TB33d
Major oxides							
SiO_2	58.96	58.48	59.26	57.69	52.17	52.77	52.86
TiO_2	0.97	1.01	0.97	0.97	1.05	0.55	0.58
Al_2O_3	16.62	15.80	16.60	16.75	17.07	18.80	18.69
TFe_2O_3	6.44	6.95	6.68	6.47	8.46	7.44	7.04
MnO	0.10	0.09	0.10	0.10	0.13	0.14	0.13
MgO	3.36	3.12	3.18	3.55	5.57	5.55	5.54
CaO	5.47	5.22	5.11	5.79	8.08	8.03	8.57
Na_2O	3.69	3.83	3.59	3.65	3.86	4.03	4.18
K_2O	3.10	3.21	3.31	3.06	2.23	1.32	0.64
P_2O_5	0.26	0.29	0.26	0.27	0.31	0.16	0.14
$Mg^{\#}$	0.51	0.47	0.49	0.52	0.57	0.60	0.61
Na_2O/K_2O	1.19	1.19	1.08	1.19	1.73	3.05	6.51
LOI	1.02	1.64	0.95	1.04	1.25	0.81	1.32
Total	99.99	99.65	100.03	99.34	100.19	99.59	99.69
Trace element							
Sc	13.2	14.6	13.8	14.1	16.8	20.8	24.2
V	138	143	136	144	220	165	203
Cr	50.0	45.0	43.0	55.0	86.0	18.0	23.0
Co	16.9	20.5	17.5	15.8	23.8	14.4	14.1
Ni	27.0	41.0	27.0	31.0	48.0	11.0	12.0
Cu	74.7	336	79.0	49.3	78.3	46.6	30.2
Zn	72.1	70.2	73.4	73.3	111	66.6	80.5
Ga	17.0	16.6	18.3	17.2	16.8	13.7	17.0
Ge	1.37	1.22	1.25	1.40	1.22	1.21	1.48
Rb	91.4	102	87.1	82.4	41.3	42.4	20.2
Sr	716	693	735	762	937	656	745
Y	16.0	17.5	16.6	15.8	13.4	10.5	10.8
Zr	143	97	127	155	57	43	41
Nb	7.6	8.3	8.2	7.1	4.0	0.8	1.2
Ba	366	357	437	393	297	144	128
La	28.3	30.0	29.9	27.3	20.2	8.30	11.3
Ce	59.5	62.2	62.3	56.7	42.4	18.1	22.4
Pr	7.41	7.83	7.74	7.19	5.54	2.55	2.92
Nd	29.2	30.8	30.4	28.2	21.9	11.2	12.4
Sm	5.05	5.48	5.24	4.84	4.03	2.37	2.50
Eu	1.29	1.30	1.32	1.28	1.28	0.85	1.04
Gd	3.99	4.29	4.07	3.84	3.28	2.05	2.25
Tb	0.57	0.63	0.59	0.54	0.48	0.32	0.35
Dy	3.02	3.32	3.12	3.04	2.58	1.91	2.01
Ho	0.57	0.63	0.59	0.58	0.50	0.39	0.41
Er	1.56	1.72	1.65	1.54	1.35	1.11	1.17
Tm	0.23	0.25	0.24	0.23	0.19	0.17	0.18
Yb	1.44	1.53	1.49	1.41	1.20	1.06	1.16
Lu	0.22	0.24	0.23	0.22	0.19	0.18	0.18
Hf	3.52	2.50	3.22	3.85	1.61	1.21	1.17
Ta	0.52	0.60	0.54	0.44	0.26	0.05	0.08
Th	12.1	14.0	10.9	7.19	3.25	0.75	1.77
U	2.72	2.42	2.69	1.87	0.89	0.23	0.53
Th/La	0.43	0.47	0.36	0.26	0.16	0.09	0.16
Sr/Y	45	40	44	48	70	63	69
La/Yb	20	20	20	19	17	8	10
Zr/Sm	28	18	24	32	14	18	16

LOI = Loss on ignition; $Mg^{\#} = 100 \times$ molar $Mg^{2+}/(Mg^{2+} + \text{total } Fe^{2+})$.

Table 3
Sr–Nd isotope data of the Kelu intrusive rocks in southern Tibet.

Sample	$^{87}Rb/^{86}Sr$	$^{87}Sr/^{86}Sr$	2σ	$(^{87}Sr/^{86}Sr)_i$	$^{147}Sm/^{144}Nd$	$^{147}Nd/^{144}Nd$	2σ	$(^{147}Nd/^{144}Nd)_i$	$\varepsilon_{Nd}(t)$	T_{DM} (Ma)	T_{2DM} (Ma)
07TB33a-1	0.369	0.704298	0.000013	0.7038	0.105	0.512753	0.000010	0.512688	3.4	557	622
07TB33a-2	0.128	0.704147	0.000010	0.7040	0.111	0.512740	0.000011	0.512671	3.0	612	649
07TB33b-2	0.343	0.704272	0.000017	0.7038	0.104	0.512768	0.000009	0.512703	3.7	534	598
07TB33d	0.0785	0.704224	0.000017	0.7041	0.122	0.512816	0.000009	0.512740	4.4	559	539
07TB33e	0.313	0.704273	0.000017	0.7039	0.104	0.512778	0.000010	0.512713	3.9	519	581

$(^{87}Sr/^{86}Sr)_i = (^{87}Sr/^{86}Sr)_i - (^{87}Rb/^{86}Sr)_i \times (e^{\lambda t} - 1)$; $^{87}Rb/^{86}Sr = (Rb/Sr) \times 2.8956$; $\lambda_{Rb-Sr} = 0.0142\ Ga^{-1}$
$(^{143}Nd/^{144}Nd)_i = (^{143}Nd/^{144}Nd)_i - (^{147}Sm/^{144}Nd)_i \times (e^{\lambda T} - 1)$; $^{147}Sm/^{144}Nd = (Sm/Nd) \times 0.60456$; $\lambda_{Sm-Nd} = 0.00654\ Ga^{-1}$
$\varepsilon_{Nd}(t) = [(^{143}Nd/^{144}Nd)_i(t)/(^{143}Nd/^{144}Nd)_{iHUR}(t) - 1] \times 10^4$; $(^{143}Nd/^{144}Nd)_{iHUR}(t) = 0.512638 - 0.1967 \times (e^{\lambda t} - 1)$
$T_{DM} = 1/\lambda \times \ln\{1 + [((^{143}Nd/^{144}Nd)_i - 0.51315)/((^{147}Sm/^{144}Nd)_i - 0.2137)]\}$
$T_{2DM} = 1/\lambda \times \ln\{1 + [(^{143}Nd/^{144}Nd)_i - ((^{147}Sm/^{144}Nd)_i - 0.118) \times (e^{\lambda t} - 1) - 0.51315]/(0.118 - 0.2137)\}$.

Table 4
Zircon Lu–Hf isotope data for the Kelu intrusive rocks (sample 07TB33b-2) in southern Tibet.

Spot	$^{176}Yb/^{177}Hf$	$^{176}Lu/^{177}Hf$	$^{176}Hf/^{177}Hf$	2σ	$\varepsilon_{Hf}(t)$	2σ	T_{DM}	$f_{Lu/Hf}$
1	0.059476	0.001693	0.283089	0.000034	13.2	1.2	234	−0.95
2	0.064349	0.001997	0.283094	0.000031	13.3	1.1	229	−0.94
3	0.051463	0.001704	0.283035	0.000032	11.2	1.1	313	−0.95
4	0.063766	0.002012	0.283064	0.000039	12.2	1.4	274	−0.94
5	0.049938	0.001587	0.283043	0.000045	11.5	1.6	301	−0.95
6	0.046527	0.001490	0.283038	0.000030	11.4	1.1	307	−0.96
7	0.073806	0.002424	0.283061	0.000037	12.1	1.3	281	−0.93
8	0.064205	0.002172	0.283091	0.000038	13.2	1.3	234	−0.93
9	0.088089	0.003024	0.283090	0.000061	13.1	2.1	242	−0.91
10	0.028721	0.001022	0.283162	0.000050	15.8	1.8	126	−0.97
11	0.020097	0.000741	0.283114	0.000046	14.1	1.6	194	−0.98
12	0.017131	0.000650	0.282978	0.000050	9.3	1.8	386	−0.98
13	0.036518	0.001322	0.283112	0.000037	14.0	1.3	199	−0.96
14	0.059476	0.001693	0.283089	0.000034	13.2	1.2	234	−0.95

$\varepsilon_{Hf}(t) = 10^4 \times \{[(^{176}Hf/^{177}Hf)_i - (^{176}Lu/^{177}Hf)_i \times (e^{\lambda t} - 1)]/[(^{176}Hf/^{177}Hf)_{iHUR,0} - (^{176}Lu/^{177}Hf)_{iHUR} \times (e^{\lambda t} - 1)] - 1\}$
$T_{DM} = 1/\lambda \times \ln\{1 + [(^{176}Hf/^{177}Hf)_i - (^{176}Hf/^{177}Hf)_{iM}]/[(^{176}Lu/^{177}Hf)_i - (^{176}Lu/^{177}Hf)_{iM}]\}$
$f_{Lu/Hf} = (^{176}Lu/^{177}Hf)_i/(^{176}Lu/^{177}Hf)_{iHUR} - 1$, where $\lambda = 1.867 \times 10^{-11}$ year^{-1} (Söderlund et al., 2004); $(^{176}Lu/^{177}Hf)_i$ and $(^{176}Hf/^{177}Hf)_i$ are the measured values of the samples; $(^{176}Lu/^{177}Hf)_{iHUR} = 0.0332$ and $(^{176}Lu/^{177}Hf)_{iHUR,0} = 0.282772$ (Blichert-Toft and Albarede, 1997); $(^{176}Lu/^{177}Hf)_{iM} = 0.0384$ and $(^{176}Lu/^{177}Hf)_{iM} = 0.28325$ (Griffin et al., 2000).

+15.8) (Table 4) (Fig. 6a and b). We note the remarkable feature of Hf–Nd isotope decoupling in the Kelu quartz monzonite (Fig. 6c).

5. Discussions

5.1. Petrogenesis

Adakites were usually considered to be derived by partial melting of subducted oceanic crust (Defant and Drummond, 1990; Rapp et al., 1999; Defant et al., 2002; Martin et al., 2005; Escuder et al., 2007; Wang et al., 2007a, 2008a; Manikyamba et al., 2009; Zhu et al., 2009; Tang et al., 2010). Other models were also proposed to account for the genesis of the intermediate-acid rocks with geochemical characteristics similar to adakites (i.e., adakitic rocks): (a) crustal assimilation and fractional crystallization (AFC) process from parental basaltic magmas (Castillo et al., 1999; Macpherson et al., 2006); (b) mixing of felsic and basaltic magmas (Guo et al., 2007a, 2009; Streck et al., 2007); (c) melting of thickened or delaminated lower crust (Atherton and Petford, 1993; Xu et al., 2002; Chung et al., 2003; Gao et al., 2004; Hou et al., 2004; Topuz et al., 2005; Wang et al., 2005, 2006a,b, 2007b,c; Wen et al., 2008a; Huang et al., 2008, 2009; Karsli et al., 2010; He et al., 2011); (d) melting of subducted continental crust (Wang et al., 2008b, 2010b; Xu et al., 2009). Based on geochronological and geochemical data for the Kelu quartz monzonites, we suggest that they were unlikely to have been produced by the latter four models, but by partial melting of subducted oceanic crust. Below we give the reasoning of our interpretation.

Castillo et al. (1999) proposed that adakitic rocks were generated by crustal assimilation and low pressure fractional crystallization process (involving olivine + clinopyroxene + plagioclase + hornblende + titanoagnetite) from parental basaltic magmas. The Kelu adakitic rocks do not exhibit the compositional trends produced by low pressure fractional crystallization of a hornblende-bearing assemblage as in Fig. 7a and b. In addition, high-pressure fractional crystallization (involving garnet) of hydrous basaltic melts also could not have generated the Kelu adakitic rocks as adakitic rocks generated by such a process generally exhibit distinct geochemical trends (Macpherson et al., 2006), e.g., Dy/Yb and Sr/Y ratios increase with increasing SiO_2 contents, which are not observed in the Kelu adakitic rocks (Fig. 7c and d). Therefore, the Kelu adakitic rocks could not have been derived by fractional crystallization.

It is also unlikely that the Kelu adakitic rocks were generated by magma mixing of felsic and basaltic magmas. Generally, magma mixing produces straight arrays in binary plot on major and trace elements (Macpherson et al., 2006), but the La and Na_2O versus SiO_2 plots of the Kelu adakitic rocks (Fig. 7a and b) do not display such straight arrays. In addition, the Kelu felsic quartz monzonites (adakitic rocks) have lower $(^{87}Sr/^{86}Sr)_i$, and similar $\varepsilon_{Nd}(t)$, values compared to the Kelu mafic diorites (Fig. 7e and f), indicating that the Kelu adakitic rocks could not have been generated by magma mixing. Moreover, the absence of Hf isotopic compositional variation from rims to cores of zircon grains in the Kelu adakitic rocks is inconsistent with magma mixing (Yang et al., 2006, 2007).

Adakitic rocks generated by partial melting of delaminated lower crust or subducted continental crust usually exhibit relatively low and negative $\varepsilon_{Nd}(t)$ and slightly high $(^{87}Sr/^{86}Sr)_i$ values (Fig. 5a) (Xu et al., 2002; Wang et al., 2006b, 2008b; Xu et al., 2009). However, the Kelu adakitic rocks exhibit high and positive $\varepsilon_{Nd}(t)$ and slightly low $(^{87}Sr/^{86}Sr)_i$ values (Fig. 5a). Although it is possible that the delaminated or subducted juvenile crust-derived

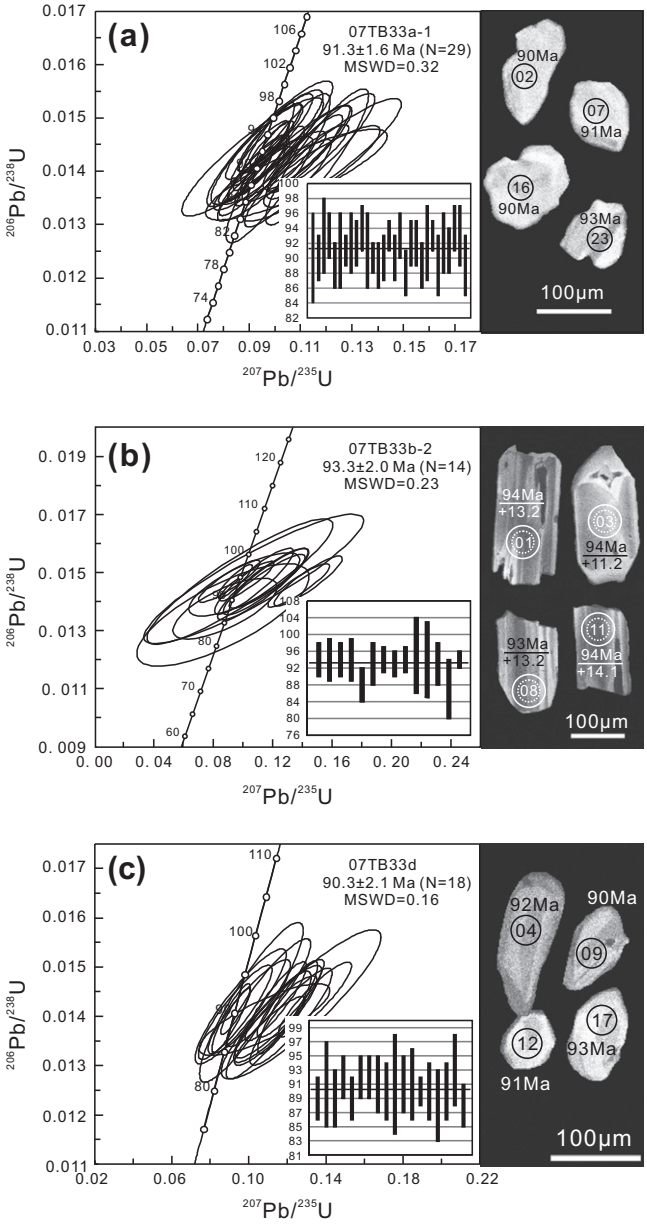

Fig. 2. LA–ICP–MS U–Pb zircon concordia diagram with Cathodoluminescence images for the intrusive rocks in the Kelu Cu–Au ore deposit. Solid and dashed circles indicate the locations of U–Pb age and Hf analytical sites, respectively, with numbers in the circles representing spot numbers. The age and $\varepsilon_{Hf}(t)$ value of each spot are shown.

adakitic rocks would exhibit high and positive $\varepsilon_{Nd}(t)$ and low $(^{87}Sr/^{86}Sr)_i$ values, adakitic rocks formed by delamination generally occur in a within-plate extensional setting (Xu et al., 2002; Gao et al., 2004; Wang et al., 2006b). In addition, the Kelu adakitic rocks were generated in an arc rather than a collisional setting in the Cretaceous (see detailed discussion below). Therefore, we suggest that the adakitic rocks were not generated by partial melting of delaminated lower crust or subducted continental crust.

Adakitic rocks derived by partial melting of thickened mafic lower crust are usually characterized by low-MgO or -$Mg^{\#}$ values (Fig. 8a and b) and low Cr and Ni contents, which are similar to those of experimental melts from metabasalts and eclogites (mostly $Mg^{\#} < 45$) (Sen and Dunn, 1994; Rapp and Watson, 1995; Rapp et al., 1999). For example, the Late Cretaceous adakitic rocks in the eastern GBST, which have low $Mg^{\#}$ (31–37) values and peraluminous compositions (A/CNK = 1.05–1.13), are considered to

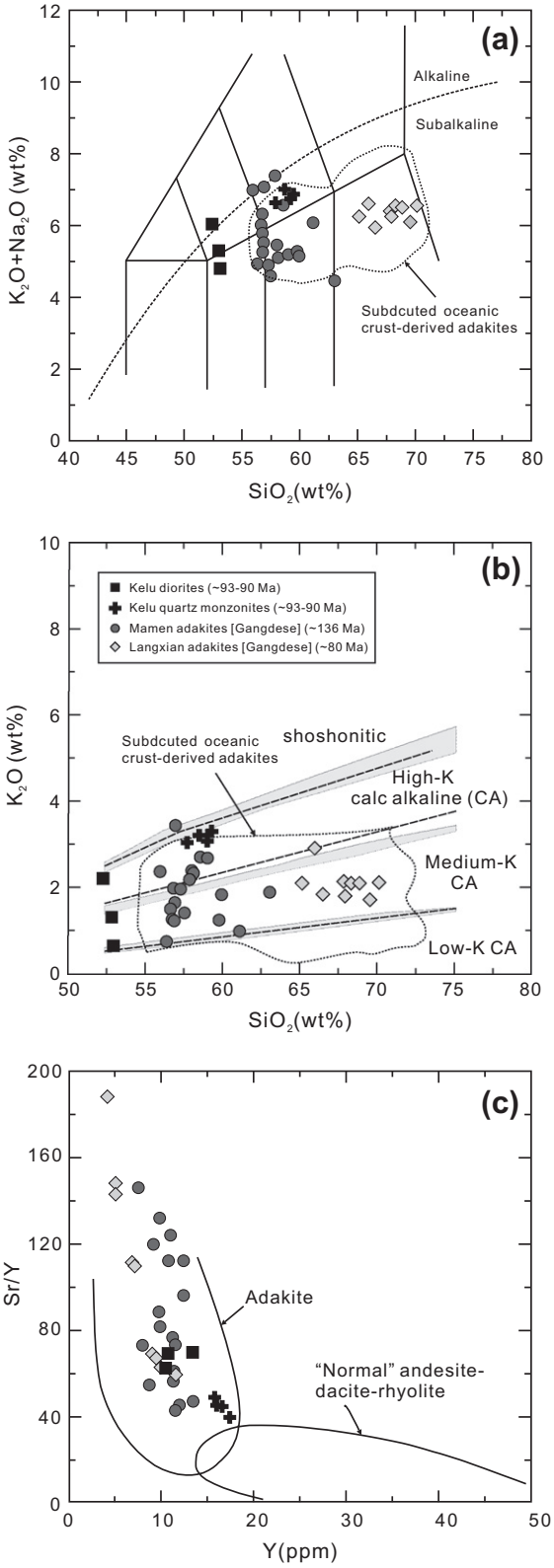

Fig. 3. (a) SiO_2 (wt.%) versus $Na_2O + K_2O$ diagram (Middlemost, 1994), (b) SiO_2 (wt.%) versus K_2O diagram (Peccerillo and Taylor, 1976), (c) Sr/Y versus Y diagram (Defant and Drummond, 1993). Data for the Mamen adakites in the Gangdese Belt are from Kang et al. (2009) and Zhu et al. (2009). Data for the Langxian adakites in the Gangdese Belt are from Wen et al. (2008a). Data for subducted oceanic crust-derived adakties are from Martin et al. (2005), and references therein.

have been generated by partial melting of thickened lower crust (e.g., Wen et al., 2008a). In contrast, the Kelu adakitic rocks have

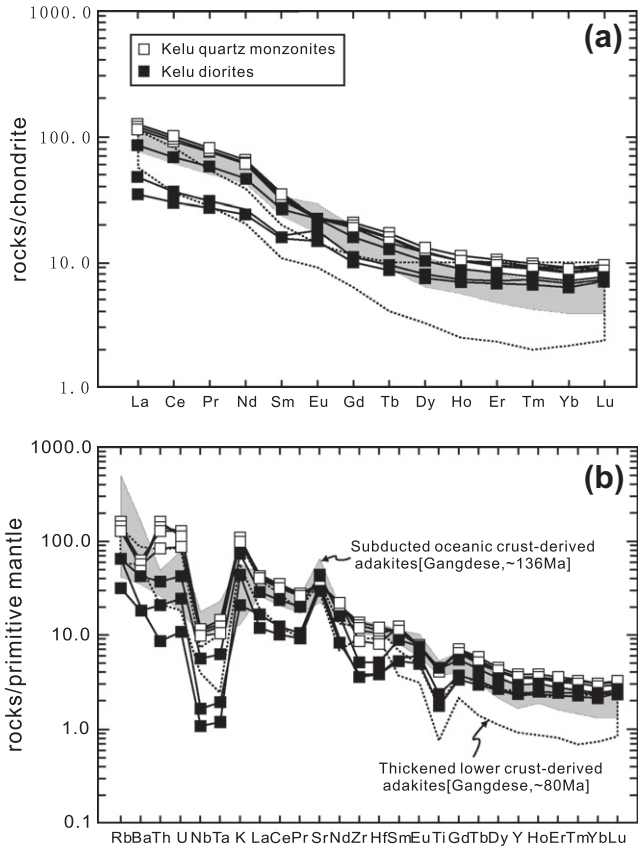

Fig. 4. (a) Chondrite-normalized REE patterns and (b) primitive mantle normalized trace element patterns for the Kelu intrusive rocks. Chondrite and primitive mantle normalizing values are from Sun and McDonough (1989). Data sources are the same as for Fig. 3.

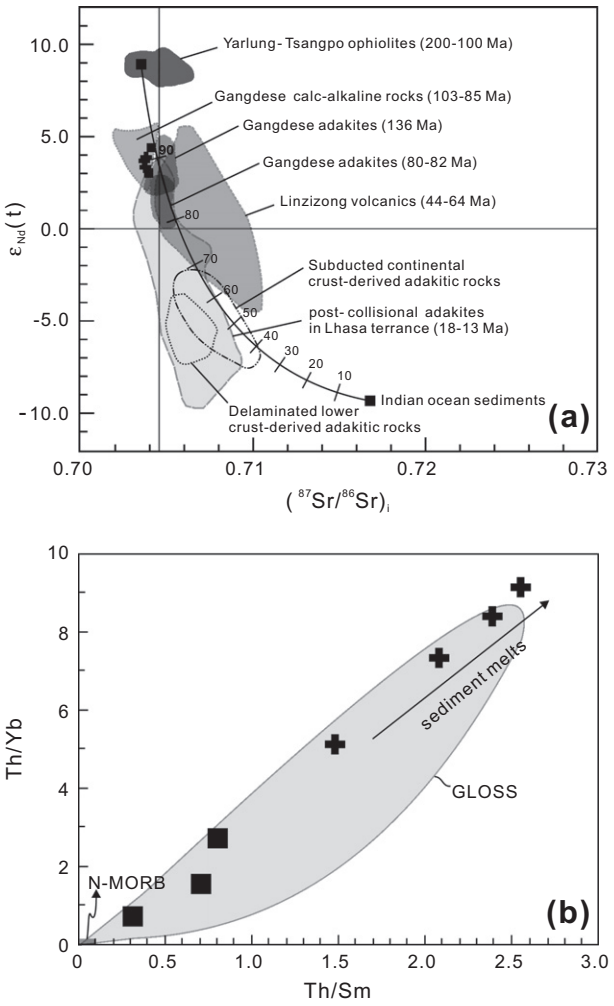

Fig. 5. (a) $\varepsilon_{Nd}(t)$ versus $(^{87}Sr/^{86}Sr)_i$ diagrams for Kelu intrusive rocks. (b) Th/Yb versus Th/Sm plot (after Guo et al. (2007b). Data for GLOSS and MORB are from Rehkamper and Hofmann (1997) and Plank and Langmuir (1998). Data sources: Yarlung Tsangpo ophiolites (Miller et al., 2003; Xu and Castillo, 2004; Zhang et al., 2005; Guilmette et al., 2009), Gangdese calc-alkaline rocks and adakites (82–80 Ma) (Wen et al., 2008a), Gangdese adakites (~136 Ma) (Zhu et al., 2009), Linzizong volcanic rocks (Mo et al., 2007, 2008), post-collisional adakites in the Lhasa Block (18–13 Ma) (Hou et al., 2004; Qu et al., 2004; Gao et al., 2007; Guo et al., 2007b), subducted continental crust-derived adakitic rocks in the Qiangtang Block (Wang et al., 2008b, 2010b), and delaminated lower crust-derived adakitic rocks in the eastern Yangtze Block (Wang et al., 2006a,b).

high $Mg^{\#}$ (47–52) and are metaluminous (A/CNK = 0.82–0.88). Commonly, adakitic $Mg^{\#}$ values higher than those of the thickened lower crust-derived adakitic rocks are interpreted as indicating melt–mantle interactions (e.g., Rapp et al., 1999). The Kelu adakitic rocks have higher $Mg^{\#}$ values than those of metabasaltic and eclogite experiment melts, indicating that they were not generated by partial melting of thickened mafic lower crust.

We suggest that the Kelu adakitic rocks were most likely generated by partial melting of subducted oceanic crust based on the following evidence:

(1) The Late Cretaceous Kelu adakitic rocks were formed in an arc setting. Based on the studies on tectonic, sedimentary basin and volcanism in the northern Lhasa Block, it has been proposed that the Cretaceous-Tertiary shortening processes and Cretaceous magmatism and syncontractional basin development in Central Tibet were the product of northward low-angle subduction of the Neo-Tethyan oceanic lithosphere and Lhasa-Qiangtang continental collision, respectively (Kapp et al., 2005, 2007; Decelles et al., 2007). Based on data for Cretaceous magmatic rocks in the eastern GBST, Wen et al. (2008a) proposed that "normal-angle" subduction occurred before ~80 Ma in southern Tibet. Accordingly, the Cretaceous adakitic rocks and associated Cu–Au deposits in the GBST are most plausibly related to the northward subduction of the Neo-Tethyan oceanic crust (Chung et al., 2005; Wen et al., 2008a,b; Ji et al., 2009a,b).

(2) The Kelu adakitic rocks have slightly high Na_2O/K_2O (1.08–1.19) and $Mg^{\#}$ (47–52) values similar to those of adakites derived by partial melting of subducted oceanic crust (Fig. 8a and b) (Defant and Drummond, 1993; Li and Li, 2003; Martin et al., 2005; Wang et al., 2007a,b,c, 2008a; Zhu et al., 2009). The slightly high MgO and $Mg^{\#}$ values of the Kelu adakitic rocks, however, suggest minor interactions between the slab-derived magmas and mantle wedge peridotites during magma ascent. In addition, the Kelu adakitic rocks exhibit trace element patterns similar to those of the ~136 Ma Mamen adakites (Fig. 4a and b), which are considered to have been derived from partial melting of subducted Neo-Tethyan oceanic crust (Zhu et al., 2009).

(3) The Kelu adakitic rocks have higher $\varepsilon_{Nd}(t)$ and lower $(^{87}Sr/^{86}Sr)_i$ values than the 80–82 Ma thickened mafic lower crust-derived adakitic rocks in the eastern GBST (Fig. 5a) (Wen et al., 2008a). Although their $\varepsilon_{Nd}(t)$ values are lower than those of Jurassic MORB distributed along the Yarlung-Tsangpo suture (Xu and Castillo, 2004; Guilmette et al., 2009), they plot in the field of the Mamen adakites in the GBST that are considered to have been derived from subducted Neo-Tethyan slabs (Fig. 5a) (Zhu et al., 2009).

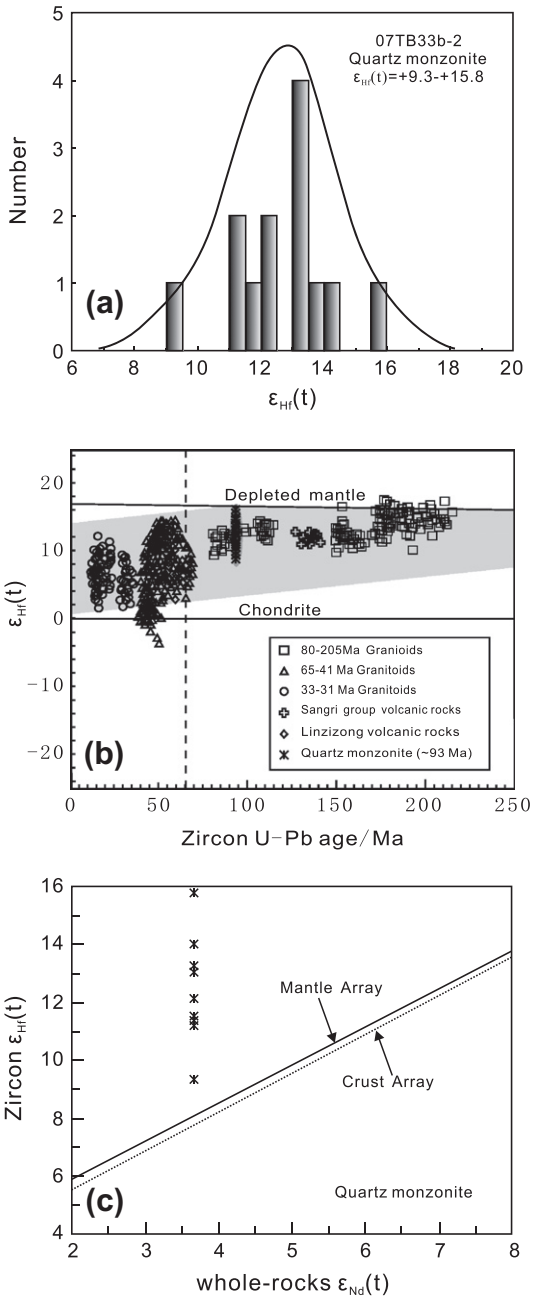

Fig. 6. (a) Histograms of $\varepsilon_{Hf}(t)$ values for zircons in the Kelu quartz monzonites and (b) zircon Hf isotopic compositions of the Gangdese batholith (after Ji et al., 2009b). (c) Zircon $\varepsilon_{Hf}(t)$ versus whole-rocks $\varepsilon_{Nd}(t)$ values for the Kelu quartz monzonite sample. Mantle and crust arrays are from Vervoort et al. (1999).

(4) Geochemical characteristics suggest that the source of the Kelu adakitic rocks contained sedimentary components in addition to basaltic oceanic crust components. On a plot of Th/Yb versus Th/Sm (Fig. 5b), the quartz monzonite samples exhibit a linear trend consistent with those of oceanic sediment melts (Elburg et al., 2002; Guo et al., 2007b). In addition, the Sr–Nd isotopic compositions of the Kelu adakitic rocks (Fig. 5a) are consistent with generation by partial melting of ~90% basaltic oceanic crust and ~10% oceanic sediments.

(5) The Kelu adakitic rocks exhibit a clear Hf–Nd isotope decoupling (Fig. 6c). Commonly, garnet has the greatest potential for decoupling neodymium and hafnium isotopic systems (Johnson et al., 1996; Vervoort and Jonathan Patchett, 1996; Schmitz et al., 2004). Owing to the large partition coefficients of garnet for Lu compared to Sm, Nd and Hf, residual garnet at the source of magmatic rocks has a large potential for retaining Lu over time, and producing high $^{176}Hf/^{177}Hf$ reservoirs in melt. Therefore, magmas derived from such garnet-bearing residual assemblages may be high in $^{176}Hf/^{177}Hf$ relative to $^{143}Nd/^{144}Nd$. As garnet is mainly a residual phase in the source during the generation of adakitic magmas by partial melting of subducted oceanic crust (Defant and Drummond, 1990; Martin, 1999; Xiong et al., 2006; Xiong, 2006b), the Kelu adakitic magmas derived from such a source should contain Hf–Nd isotope compositions similar to their source. However, some sediments (e.g., terrigenous and hydrogenetic clays) commonly exhibit decoupled behavior of Hf and Nd because the low Lu/Hf zircons mainly are saved in the residual weathered source but the resulting terrigenous and hydrogenetic clay, with anomalously radiogenic Hf, are delivered to the ocean (Vervoort et al., 1999, 2011). Partial melting of subducted oceanic crust as well as some oceanic sediments with anomalously radiogenic Hf may result in anomalously high $\varepsilon_{Hf}(t)$ values relative to the whole-rocks $\varepsilon_{Nd}(t)$ values of the resulting melts (i.e., adakitic magmas). For example, similar ranges of zircon $\varepsilon_{Hf}(t)$ at a given whole-rock $\varepsilon_{Nd}(t)$ are reported for I-type granites of the Lachlan Fold Belt in Australia by Hawkesworth and Kemp (2006). In that case, however, the granites are not adakitic and the sediment component is considered to have been contributed to the magmas within the crust. In the case of the Kelu adakitic rocks, minor sediments in the source likely caused similar pronounced Hf–Nd isotope decoupling (Figs. 5a and 6c).

We thus conclude that the Kelu adakitic (quartz monzonite) magmas were most likely derived by partial melting of subducted Neo-Tethyan basaltic oceanic crust and minor sediments, and subsequently underwent minor interactions with mantle wedge peridotite (Fig. 9). Previous studies on the Xigaza ophiolites suggest that the Neo-Tethyan Ocean was opened in the Early Cretaceous (~130–120 Ma) (Allègre and Xu, 1984; Malpas et al., 2003; Wang et al., 2006c; Guilmette et al., 2009). When such oceanic curst was subducted during the Late Cretaceous (~90 Ma), it is possible that partial melting of relatively young oceanic crust generated adakitic magmas (e.g., Defant and Drummond, 1990). Moreover, the Kelu adakites were coeval with charnockites with adakitic affinities from the eastern Gangdese area, which were considered to have resulted from the northward subduction of the Neo-Tethyan mid-oceanic ridge beneath the Gangdese Belt (Zhang et al., 2010). In addition, as suggested in Peacock et al. (1994), in most subduction zones, substantial partial melting of old subducting oceanic crust will occur if high shear stresses (>~100 MPa) can be maintained by rocks close to, or above, their melting temperatures (>750 °C).

The Kelu diorites exhibit low SiO_2 and high MgO or $Mg^{\#}$ (Table 2), similar to magnesian andesites in arc settings (Kay, 1978; Polat and Kerrich, 2002; Escuder et al., 2007; Wang et al., 2008a). Their geochemical characteristics are similar to those of adakites (Fig. 3c). Magnesian andesites associated with subducted oceanic crust-derived adakites are generally considered to have been the product of hybridization of adakitic melt with mantle peridotites (Polat and Kerrich, 2002; Calmus et al., 2003; Escuder et al., 2007; Wang et al., 2008a; Manikyamba et al., 2009). In addition, the diorites samples exhibit some obvious variations in LREE, Sr, V, Cr and Ni contents. For example, two diorite samples (07TB33c-1, 07TB33d) have lower LREE and Sr contents than another diorite sample (07TB33a-2) (Fig. 4; Table 2). In general, the apatites from the I-type Gangdese granitoids exhibit the most markedly LREE-

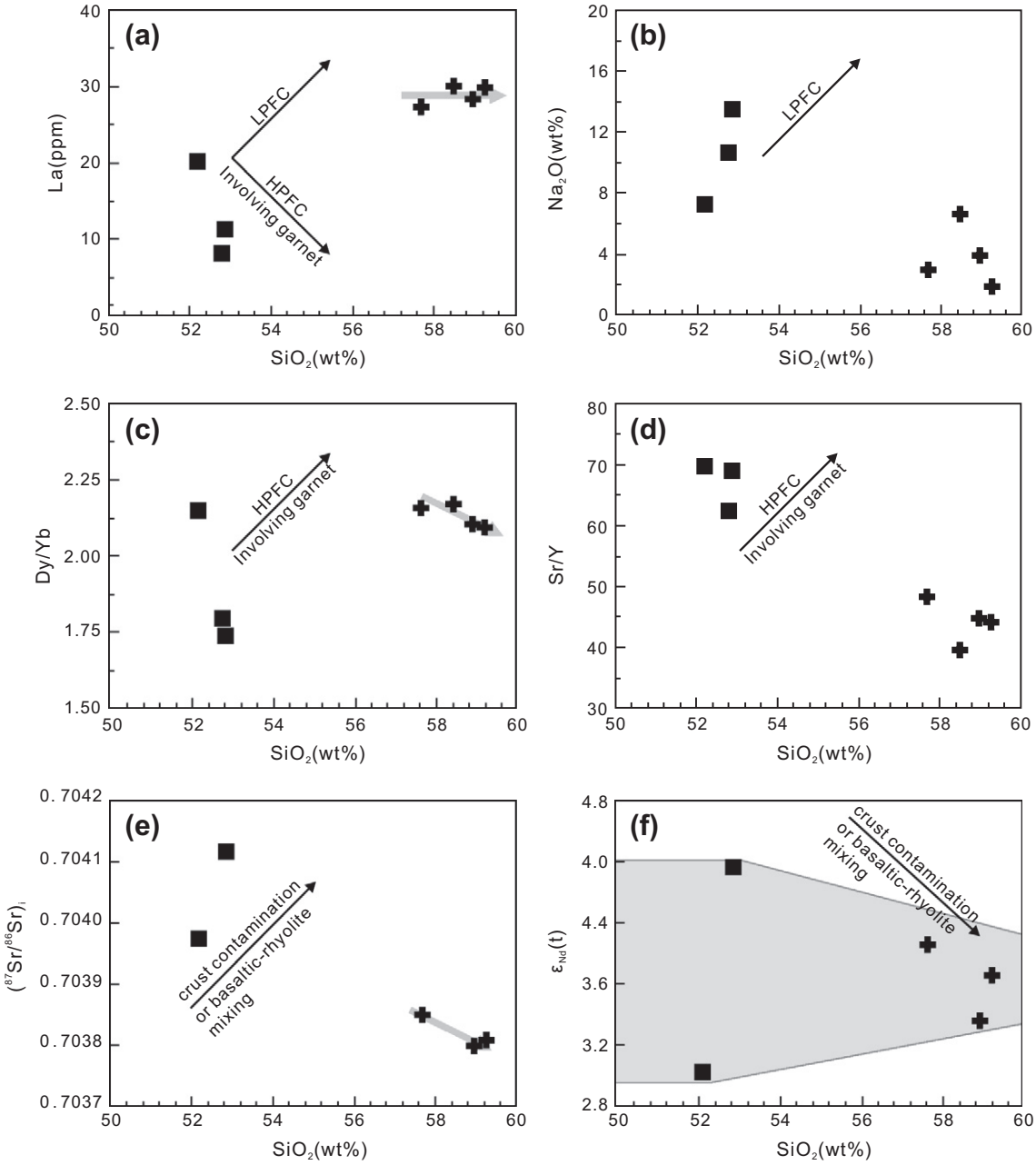

Fig. 7. Plots of (a) SiO_2 versus La; (b) SiO_2 versus Na_2O; (c) SiO_2 versus Dy/Yb; (d) SiO_2 versus Sr/Y; (e) SiO_2 versus $(^{87}Sr/^{86}Sr)_i$; and (f) SiO_2 versus $\varepsilon_{Nd}(t)$ for the Kelu intrusive rocks. Fractional crystallization trends in a–d: HPFC, high-pressure fractional crystallization involving garnet (Macpherson et al., 2006); LPFC, low-pressure fractional crystallization involving olivine + clinopyroxene + plagioclase + hornblende + titanomagnetite (Castillo et al., 1999).

enriched patterns (Chu et al., 2009). Moreover, strontium is more compatible in apatite than melt (Watson and Green, 1991; Sha and Chappell, 1999). Therefore, the LREE depletion and the decrease in Sr contents (Fig.4) are possibly related to the fractionation of minor apatite. The diorite samples also exhibit more variable V, Cr and Ni contents than the adakitic quartz monzonite samples (Table 2). Moreover, the diorite sample (07TB33c-1) with the lowest V, Cr and Ni contents has the highest Zr/Sm ratio among three diorite samples (Table 2). Due to the incompatibility of Zr and compatibility of Sm and V in hornblende (e.g., Drummond et al., 1996), its fractional crystallization will cause the increasing of Zr/Sm ratios and the decreasing of V in residual magmas. Therefore, we suggest that the Kelu diorites associated with slab-derived adakitic quartz monzonites were most likely derived from extensive interactions between ascending siliceous slab-melts and mantle wedge peridotites, with the fractionation of some apatite and hornblende.

5.2. Implications for Cu–Au mineralization

Since Thiéblemont et al. (1997) and Sajona and Maury (1998) reported that epithermal and porphyry Cu–Au deposits are closely associated with Cenozoic adakites in the Philippines arc, numerous subsequent other workers have reported Cu–Au–Mo deposits associated with adakitic rocks in various parts of the world (e.g., Chile, Mexico, Ecuador, China and southwestern United States), although in some cases the origin of the adakitic signature has been strongly debated (McInnes and Cameron, 1994; Skewes and Stern, 1994; Thiéblemont et al., 1997; Sajona and Maury, 1998; Kay and Mpodozis, 2001; Oyarzun et al., 2001; González-Partida et al., 2003;

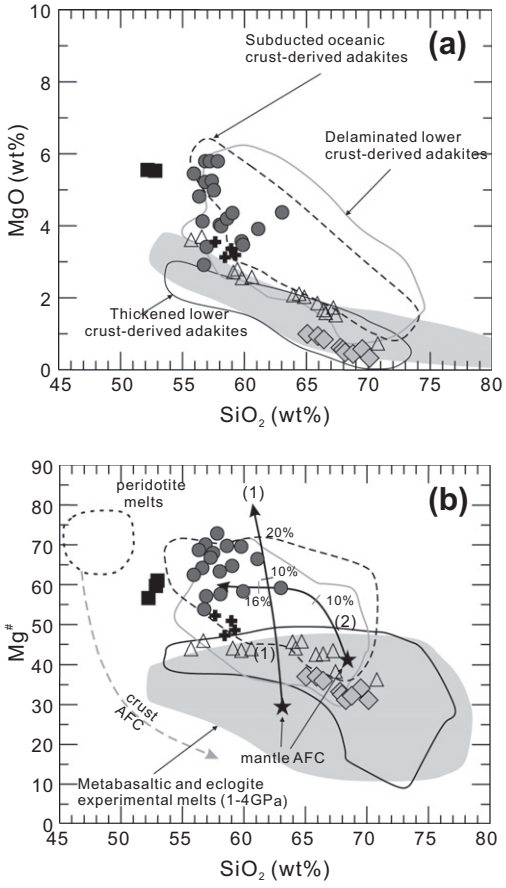

Fig. 8. (a) SiO_2 versus MgO diagram and (b) SiO_2 versus $Mg^{\#}$ digram for the Kelu intrusive rocks. Mantle AFC curves, with proportions of assimilated peridotite indicated, are after Stern and Kilian (1996) (Curve 1) and Rapp et al. (1999) (Curve 2). Peridotite melts and crust AFC curves are from Stern and Kilian (1996). Data for metabasaltic and eclogite experimental melts (1–4.0 GPa), and peridotite-hybridized equivalents, are from Rapp et al. (1999) and references therein. The field for subducted oceanic crust-derive adakites, and delaminated or thickened lower crust-derived adakitic rocks are from Wang et al. (2006a,b, 2007a,b,c). Data sources and symbols are the same as in Fig. 3.

Reich et al., 2003; Cooke et al., 2005; Wang et al., 2006a,b, 2007c; Richards and Kerrich, 2007; Chiaradia et al., 2009; Hou et al., 2009; Liu et al., 2010a,b; Sun et al., 2010; Tang et al., 2010). The three largest super-giant porphyry Cu–Au deposits in the world, i.e., the E1 Teniente, Chuquicamata and Río Blanco–Los Bronces deposits, all occur in the central Andes arc and are considered by many workers to have been related to the adakites derived by partial melting of subducted oceanic crust (Skewes and Stern, 1994; Oyarzun et al., 2001; Reich et al., 2003; Cooke et al., 2005).

Subduction zones have been considered as uniquely favorable tectonic settings for the generation of Cu–Au deposits (Oyarzun et al., 2001; Defant et al., 2002; Reich et al., 2003). The upper part of subducted oceanic crust has very high intrinsic fO_2 due to equilibration with seawater during hydrothermal alteration and the deposition of terrigenous sediments (Mungall, 2002). Melts with high Fe_2O_3 content derived from the slab thus have the unique ability of carrying this oxidizing potential up into the overlying mantle and destabilizing mantle metal sulfides to release chalcophile Cu and Au that are mainly hosted in sulfides (Mungall, 2002). In addition, it has also been proposed that metallogenic materials (chalcophile elements) are abundant in sudducted oceanic crust (Ling et al., 2009; Liu et al., 2010a,b; Sun et al., 2010). As a result, slab-derived adakites are now recognized to be particularly prospective for Cu–Au mineralization (Defant et al., 2002).

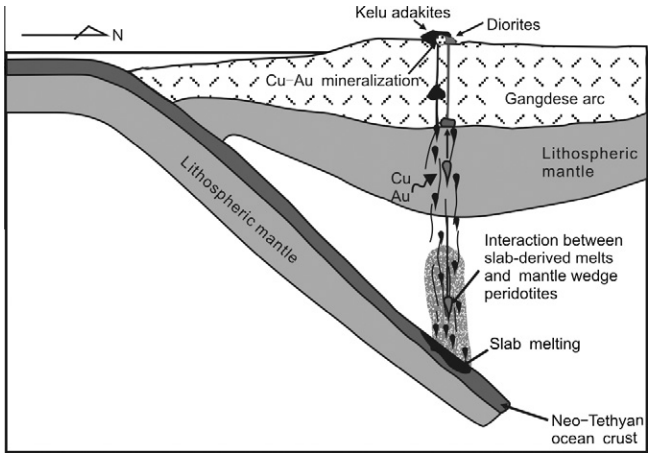

Fig. 9. A suggested model for the production of the Late Cretaceous intrusive rocks in the Kelu area.

The Kelu adakitic quartz monzonites are interpreted here as being generated by partial melting of ~90% basaltic oceanic crust and ~10% oceanic sediments with subsequent interactions between melts and the mantle wedge peridotites. The Kelu diorites are interpreted as being generated by extensive interactions between ascending siliceous slab-melts and mantle wedge peridotites. We therefore suggest that the Kelu adakitic quartz monzonites and mafic diorites should be particularly suitable for Cu–Au mineralization because: (a) their source (subducted oceanic crust) possibly contained abundant chalcophile elements (Cu and Au), and the slab-derived magmas went through the mantle, also enriched in Cu and Au sulfides; (b) the high oxygen fugacity inherited from the source (subducted oceanic crust and sediments) could have caused the decomposition of Cu and Au sulfides in the mantle to release Cu and Au (Mungall, 2002).

Previous studies have shown that Cu–Au porphyry mineralization mainly occurs in the mid-Miocene (18–10 Ma) in the GBST and is temporally and spatially associated with coeval adakitic rocks during the intra-continental convergence stage after the collision between the Indian and the Asian continents (Hou et al., 2009). Chung et al. (2003) and Hou et al. (2004) suggested that these ore-bearing adakitic porphyries were derived by partial melting of thickened mafic lower continental crust, but other researchers have suggested that they could also have been generated by other mechanisms (e.g., partial melting of residual oceanic crust, enriched mantle, or subduction-modified lower crust) (Qu et al., 2004; Gao et al., 2007; Guo et al., 2007b). As previously noted, most porphyry Cu–Au deposits in the world are formed in arc settings. Therefore, the geological settings for the mid-Miocene porphyry deposits in the GBST are somewhat different from that of classic porphyry Cu–Au deposits elsewhere in the world. On the other hand, Jurassic–Early Tertiary arc magmatic rocks are widespread in the GBST, including some Early Cretaceous subducted oceanic crust-derived adakites (Zhu et al., 2009). The Kelu adakites are associated with the first known Cretaceous Cu–Au mineralization in the GBST arc but are geodynamically related to porphyry copper–gold-hosting Jurassic (~172 Ma) arc magmatic rocks in the GBST (Tafti et al., 2009). We thus speculate that the widespread Jurassic–Early Tertiary arc magmatic rocks in the GBST may hold more potential for Cu–Au mineralization than is presently recognized.

6. Conclusions

Late Cretaceous (~90 Ma) intrusive rocks and associated Cu–Au mineralization in the Kelu area were generated in an arc setting.

These intrusive rocks consist of quartz monzonites and diorites and show geochemical characteristics of adakites. The quartz monzonites were derived by partial melting of subducted Neo-Tethyan oceanic crust and minor sediments. The diorites were most likely produced by interactions between slab melts and mantle wedge peridotite. The close association of the Late Cretaceous adakitic intrusive rocks and Cu–Au mineralization in the Kelu area suggests that the widespread arc magmatic rocks in the GBST may hold great potential for Cu–Au exploration.

Acknowledgements

We sincerely thank Professors B.M. Jahn and S.L. Chung and an anonymous reviewer for their constructive and helpful reviews on this manuscript. The work was supported by grants from the Chinese Academy of Sciences (KZCX2-YW-Q09-05-01), the Major State Basic Research Program of People's Republic of China (No. 2009CB421004) and the National Natural Science Foundation of China (Grant Nos. 41025006, 41073029 and 41121002). Hengxiang Yu, Guangqian Hu, Jinlong Ma, Ying Liu, Xiangling Tu and Xirong Liang are thanked for their assistance with laboratory and fieldwork. This is contribution No. IS-#1474 from GIGCAS, TIGeR publication #413, and contribution 166 from the ARC Centre of Excellence for Core to Crust Fluid Systems (http://www.ccfs.mq.edu.au).

References

Allègre, C.J., Xu, R.H., 1984. Lead isotopic study of the Xigaze ophiolite (Tibet): the problem of the relationship between magmatites (gabbros, dolerites, lavas) and tectonites (harzburgites). Earth and Planetary Science Letters 69, 301–310.

Akira, I., 2002. Metallogenesis of porphyry Cu deposits of the western Luzon arc, Philippines: K-Ar ages, SO_3 contents of microphenocrystic apatite and significance of intrusive rocks. Resource Geology 52, 147–161.

Andersen, T., 2002. Correction of common lead in U-Pb analyses that do not report ^{204}Pb. Chemical Geology 192, 59–79.

Atherton, M.P., Petford, N., 1993. Generation of sodium-rich magmas from newly underplated basaltic crust. Nature 362, 144–146.

Belousova, E.A., Griffin, W.L., O'Reilly, S.Y., Fisher, N.I., 2002. Igneous zircon: trace element composition as an indicator of source rock type. Contributions to Mineralogy and Petrology 143, 602–622.

Blichert-Toft, J., Albarede, F., 1997. The Lu-Hf isotope geochemistry of chondrites and the evolution of the mantle-crust system. Earth and Planetary Science Letters 148, 243–258.

Calmus, T., Aguillón-Robles, A., Maury, R.C., Bellon, H., Benoit, M., Cotten, J., Bourgois, J., Michaud, F., 2003. Spatial and temporal evolution of basalts and magnesian andesites (''bajaites'') from Baja California, Mexico: the role of slab melts. Lithos 66, 77–105.

Castillo, P.R., Janney, P.E., Solidum, R.U., 1999. Petrology and geochemistry of Camiguin Island, southern Philippines: insights to the source of adakites and other lavas in a complex arc setting. Contributions to Mineralogy and Petrology 134, 33–51.

Chen, J.S., Huang, B.C., Sun, L.S., 2010. New constraints to the onset of the India-Asia collision: Paleomagnetic reconnaissance on the Linzizong Group in the Lhasa Block, China. Tectonophysics 489, 189–209.

Chiaradia, M., Merino, D., Spikings, R., 2009. Rapid transition to long-lived deep crustal magmatic maturation and the formation of giant porphyry-related mineralization (Yanacocha, Peru). Earth and Planetary Science Letters 288, 505–515.

Chu, M.F., Wang, K.L., Griffin, W.L., Chung, S.L., O'Reilly, S.Y., Pearson, N.J., Iizuka, Y., 2009. Apatite composition: tracing petrogenetic processes in Transhimalayan Granitoids. Journal of Petrology 50, 1829–1855.

Chung, S.L., Lo, C.H., Lee, T.Y., Zhang, Y., Xie, Y., Li, X., Wang, K.L., Wang, P.L., 1998. Diachronous uplift of the Tibetan plateau starting 40 Myr ago. Nature 394, 769–773.

Chung, S.L., Liu, D.Y., Ji, J.Q., Chu, M.F., Lee, H.Y., Wen, D.J., Lo, C.H., Lee, T.Y., Qian, Q., Zhang, Q., 2003. Adakites from continental collision zones: melting of thickened lower crust beneath southern Tibet. Geology 31, 1021–1024.

Chung, S.L., Chu, M.F., Zhang, Y.Q., Xie, Y.W., Lo, C.H., Lee, T.Y., Lan, C.Y., Li, X.H., Zhang, Q., Wang, Y.Z., 2005. Tibetan tectonic evolution inferred from spatial and temporal variations in post-collisional magmatism. Earth-Science Reviews 68, 173–196.

Chung, S.L., Chu, M.F., Ji, J., O'Reilly, S.Y., Pearson, N.J., Liu, D.Y., Lee, T.Y., Lo, C.H., 2009. The nature and timing of crustal thickening in Southern Tibet: geochemical and zircon Hf isotopic constraints from postcollisional adakites. Tectonophysics 477, 36–48.

Cooke, D.R., Hollings, P., Walshe, J.L., 2005. Giant porphyry deposits: characteristics, distribution, and tectonic controls. Economic Geology 100, 801–818.

DeCelles, P.G., Kapp, P., Ding, L., Gehrels, G.E., 2007. Late Cretaceous to mid-Tertiary basin evolution in the central Tibetan Plateau: changing environments in response to tectonic partitioning, aridifi cation, and regional elevation gain. Geological Society of America Bulletin 119, 654–680.

Defant, M.J., Drummond, M.S., 1990. Derivation of some modern arc magmas by melting of young subducted lithosphere. Nature 347, 662–665.

Defant, M.J., Drummond, M.S., 1993. Mount St. Helens: potential example of the partial melting of the subducted lithosphere in a volcanic arc. Geology 21, 547–550.

Defant, M.J., Xu, J.F., Kepezhinskas, P., Wang, Q., Zhang, Q., Xiao, L., 2002. Adakites: some variations on a theme. Acta Petrologica Sinica 18, 129–142.

Ding, L., Kapp, P., Wan, X.Q., 2005. Paleocene-Eocene record of ophiolite obduction and initial India-Asia collision, south central Tibet. Tectonics 24, TC3001. http://dx.doi.org/10.1029/2004TC001729.

Ding, L., Kapp, P., Zhong, D.L., Deng, W.M., 2003. Cenozoic volcanism in Tibet: evidence for a transition from oceanic to continental subduction. Journal of Petrology 44, 1833–1865.

Drummond, M.S., Defant, M.J., Kepezhinskas, P.K., 1996. The petrogenesis of slab derived trondhjemite–tonalite–dacite/adakite magmas. Transactions of the Royal Society of Edinburgh: Earth and Environmental Science 87, 205–216.

Elburg, M.A., van Bergen, M., Hoogewerff, J., Foden, J., Vroon, P., Zulkarnain, I., Nasution, A., 2002. Geochemical trends across an arc-continent collision zone: magma sources and slab-wedge transfer processes below the Pantar Strait volcanoes, Indonesia. Geochimica et Cosmochimica Acta 66, 2771–2789.

Escuder, V.J., Contreras, F., Stein, G., Urien, P., Joubert, M., Pérez-Estaún, A., Friedman, R., Ullrich, T., 2007. Magmatic relationships and ages between adakites, magnesian andesites and Nb-enriched basalt-andesites from Hispaniola: record of a major change in the Caribbean island arc magma sources. Lithos 99, 151–177.

Gao, S., Rudnick, R.L., Yuan, H.L., Liu, X.M., Liu, Y.S., Xu, W.L., Ling, W.L., Ayers, J., Wang, X.C., Wang, Q.H., 2004. Recycling lower continental crust in the North China craton. Nature 432, 892–897.

Gao, Y.F., Hou, Z.Q., Kamber, B.S., Wei, R.H., Meng, X.J., Zhao, R.S., 2007. Adakite-like porphyries from the southern Tibetan continental collision zones: evidence for slab melt metasomatism. Contributions to Mineralogy and Petrology 153, 105–120.

Gao, Y.F., Wei, R.H., Ma, P.X., Hou, Z.Q., Yang, Z.S., 2009. Post-collisional ultrapotassic volcanism in the Tangra Yumco-Xuruco graben, south Tibet: constraints from geochemistry and Sr-Nd-Pb isotope. Lithos 110, 129–139.

Gao, Y.F., Yang, Z.S., Hou, Z.Q., Wei, R.H., Meng, X.J., Tian, S.H., 2010a. Eocene potassic and ultrapotassic volcanism in south Tibet: new constraints on mantle source characteristics and geodynamic processes. Lithos 117, 20–32.

Gao, Y.F., Yang, Z.S., Santosh, M., Hou, Z.Q., Wei, R.H., Tian, S.H., 2010b. Adakitic rocks from slab melt-modified mantle sources in the continental collision zone of southern Tibet. Lithos 119, 651–663.

González-Partida, E., Levresse, G., Carrillo-Chávez, A., Cheilletz, A., Gasquet, D., Jones, D., 2003. Paleocene adakite Au-Fe bearing rocks, Mezcala, Mexico: evidence from geochemical characteristics. Journal of Geochemical Exploration 80, 25–40.

Griffin, W.L., Pearson, N.J., Belousova, E., Jackson, S.E., van Achterbergh, E., O'Reilly, S.Y., Shee, S.R., 2000. The Hf isotope composition of cratonic mantle: LAM-MC-ICPMS analysis of zircon megacrysts in kimberlites. Geochimica et Cosmochimica Acta 64, 133–147.

Griffin, W.L., Pearson, N.J., Belousova, E.A., Saeed, A., 2006. Comment: Hf-isotope heterogeneity in zircon 91500. Chemical Geology 233, 358–363.

Guilmette, C., Hebert, R., Wang, C.S., Villeneuve, M., 2009. Geochemistry and geochronology of the metamorphic sole underlying the Xigaze Ophiolite, Yarlung Zangbo Suture Zone, South Tibet. Lithos 112, 149–162.

Guo, F., Nakamura, E., Fan, W.M., Kobayashi, K., Li, C.W., Gao, X.F., 2009. Mineralogical and geochemical constraints on magmatic evolution of Paleocene adakitic andesites from the Yanji area, NE China. Lithos 112, 321–341.

Guo, F., Nakamuru, E., Fan, W.M., Kobayoshi, K., Li, C.W., 2007a. Generation of Palaeocene Adakitic Andesites by Magma Mixing; Yanji Area, NE China. Journal of Petrology 48, 661–692.

Guo, Z.F., Wilson, M., Liu, J.Q., 2007b. Post-collisional adakites in south Tibet: products of partial melting of subduction-modified lower crust. Lithos 96, 205–224.

Hawkesworth, C.J., Kemp, A.I.S., 2006. Using hafnium and oxygen isotopes in zircons to unravel the record of crustal evolution. Chemical Geology 226 (3–4), 144–162.

He, Y., Li, S., Hoefs, J., Huang, F., Liu, S.-A., Hou, Z., 2011. Post-collisional granitoids from the Dabie orogen: new evidence for partial melting of a thickened continental crust. Geochimica et Cosmochimica Acta 75 (13), 3815–3838.

Hou, Z.Q., Cook, N.J., 2009. Metallogenesis of the Tibetan collisional orogen: a review and introduction to the special issue. Ore Geology Reviews 36, 2–24.

Hou, Z.Q., Yang, Z.M., Qu, X.M., Meng, X.J., Li, Z.Q., Beaudoin, G., Rui, Z.Y., Gao, Y.F., 2009. The Miocene Gangdese porphyry copper belt generated during post-collisional extension in the Tibetan orogen. Ore Geology Reviews 36, 25–51.

Hou, Z.Q., Gao, Y.F., Qu, X.M., Rui, Z.Y., Mo, X.X., 2004. Origin of adakitic intrusives generated during mid-Miocene east-west extension in southern Tibet. Earth and Planetary Science Letters 220, 139–155.

Huang, F., Li, S.G., Dong, F., He, Y.S., Chen, F.K., 2008. High-Mg adakitic rocks in the Dabie orogen, central China: implications for foundering mechanism of lower continental crust. Chemical Geology 255, 1–13.

Huang, X.L., Xu, Y.G., Lan, J.B., Yang, Q.J., Luo, Z.Y., 2009. Neoproterozoic adakitic rocks from Mopanshan in the western Yangtze Craton: partial melts of a thickened lower crust. Lithos 112, 367–381.
Jackson, S.E., Pearson, N.J., Griffin, W.L., Belousova, E.A., 2004. The application of laser ablation-inductively coupled plasma-mass spectrometry to in situ U-Pb zircon geochronology. Chemical Geology 211, 47–69.
Ji, W.Q., Wu, F.Y., Chung, S.L., Li, J.X., Liu, C.Z., 2009a. Zircon U-Pb geochronology and Hf isotopic constraints on petrogenesis of the Gangdese batholith, southern Tibet. Chemical Geology 262, 229–245.
Ji, W.Q., Wu, F.Y., Liu, C.Z., Chung, S.L., 2009b. Geochronology and petrogenesis of granitic rocks in Gangdese batholith, southern Tibet. Science in China Series D: Earth Sciences 52, 1240–1261.
Johnson, C.M., Shirey, S.B., Barovich, K.M., 1996. New approaches to crustal evolution studies and the origin of granitic rocks: what can the Lu∼CHf and Re∼Os isotope systems tell us? Geological Society of America Special Papers 315, 339–352.
Kang, Z.Q., Xu, J.F., Chen, J.L., Wang, B.D., 2009. Geochemistry and origin of Cretaceous adakites in Mamuxia Formation, Sangri Group, South Tibet. Geochimica 38, 334–344 (in Chinese with English abstract).
Kapp, P., Yin, A., Harrison, T.M., Ding, L., 2005. Cretaceous-Tertiary shortening, basin development, and volcanism in central Tibet. Geological Society of America Bulletin 117, 865–878.
Kapp, P., DeCelles, P.G., Gehrels, G.E., Heizler, M., Ding, L., 2007. Geologic records of the Lhasa-Qiangtang and Indo-Asian collisions in the Nima area of central Tibet. Geological Society of America Bulletin 119, 917–932.
Karsli, O., Dokuz, A., Uysal, I., Aydin, F., Kandemir, R., Wijbrans, J., 2010. Generation of the Early Cenozoic adakitic volcanism by partial melting of mafic lower crust, Eastern Turkey: implications for crustal thickening to delamination. Lithos 114, 109–120.
Kay, R.W., 1978. Aleutian magnesian andesites: melts from subducted Pacific ocean crust. Journal of Volcanology and Geothermal Research 4, 117–132.
Kay, S.M., Mpodozis, C., 2001. Central andean ore deposits linked to evolving shallow subduction systems and thickening crust. GSA Today 11, 4–9.
Lee, H.Y., Chung, S.L., Lo, C.H., Ji, J.Q., Lee, T.Y., Qian, Q., Zhang, Q., 2009. Eocene Neotethyan slab breakoff in southern Tibet inferred from the Linzizong volcanic record. Tectonophysics 477, 20–35.
Li, G.M., Qin, K.Z., Ding, K.S., Liu, T.B., Li, J.X., Wang, S.H., Jiang, S.Y., Zhang, X.C., 2006a. Geology, Ar-Ar age and mineral assemblage of Eocene skarn Cu-Au ± Mo deposits in the Southeastern Gangdese arc, Southern Tibet: implications for deep exploration. Resurce Geology 56, 315–336.
Li, W.X., Li, X.H., 2003. Adakitic granites within the NE Jiangxi ophiolites, South China: geochemical and Nd isotopic evidence. Precambrian Research 122, 29–44.
Li, X.H., Liu, D.Y., Sun, M., Li, W.X., Liang, X.R., Iiu, Y., 2004. Precise Sm-Nd and U-Pb isotopic dating of the supergiant Shizhuyuan polymetallic deposit and its host granite, Southeast China. Geological Magazine 141, 225–231.
Li, X.H., Li, Z.X., Wingate, Michael, T.D., Chung, S.L., Liu, Y., Lin, G.C., Li, W.X., 2006b. Geochemistry of the 755 Ma Mundine Well dyke swarm, northwestern Australia: part of a Neoproterozoic mantle superplume beneath Rodinia? Precambrian Research 146, 1–15.
Ling, M.X., Wang, F.Y., Ding, X., Hu, Y.H., Zhou, J.B., Zartman, R.E., Yang, X.Y., Sun, W.D., 2009. Cretaceous ridge subduction along the lower Yangtze River belt, eastern China. Economic Geology 104, 303–321.
Liu, S.A., Li, S.G., He, Y.S., Huang, F., 2010a. Geochemical contrasts between early Cretaceous ore-bearing and ore-barren high-Mg adakites in central-eastern China: implications for petrogenesis and Cu-Au mineralization. Geochimica et Cosmochimica Acta 74, 7160–7178.
Liu, Y.S., Gao, S., Hu, Z.C., Gao, C.G., Zong, K.Q., Wang, D.B., 2010b. Continental and oceanic crust recycling-induced melt–peridotite interactions in the Trans-North China Orogen: U-Pb Dating, Hf Isotopes and trace elements in zircons from mantle xenoliths. Journal of Petrology 51, 537–571.
Ludwig, K.R., 2003. User's Manual for Isoplot 3.0: A Geochronological Toolkit for Microsoft Excel. Berkeley Geochronology Center. Special Publication 4, 1–71.
Macpherson, C.G., Dreher, S.T., Thirlwall, M.F., 2006. Adakites without slab melting: high pressure differentiation of island arc magma, Mindanao, the Philippines. Earth and Planetary Science Letters 243, 581–593.
Malpas, J.G., Zhou, M.F., Robinson, P.T., Reynolds, P.H., 2003. Geochemical and geochronological constraints on the origin and emplacement of the Yarlung Zangbo ophiolites, Southern Tibet. Geological Society, London, Special Publications 218, 191–206.
Manikyamba, C., Kerrich, R., Khanna, T.C., Satyanarayanan, M., Krishna, A.K., 2009. Enriched and depleted arc basalts, with Mg-andesites and adakites: a potential paired arc–back-arc of the 2.6 Ga Hutti greenstone Block India. Geochimica et Cosmochimica Acta 73, 1711–1736.
Martin, H., 1999. Adakitic magmas: modern analogues of Archaean granitoids. Lithos 46, 411–429.
Martin, H., Smithies, R.H., Rapp, R., Moyen, J.F., Champion, D., 2005. An overview of adakite, tonalite-trondhjemite-granodiorite (TTG), and sanukitoid: relationships and some implications for crustal evolution. Lithos 79, 1–24.
McInnes, B.A., Cameron, E.M., 1994. Carbonated, alkaline hybridizing melts from a sub-arc environment: mantle wedge samples from the Tabar-Lihir-Tanga-Feni arc, Papua New Guinea. Earth and Planetary Science Letters 122, 125–141.
Middlemost, E.A.K., 1994. Naming materials in the magma/igneous rock system. Earth-Science Reviews 37, 215–224.
Miller, C., Schuster, R., Klötzli, U., Frank, W., Purtscheller, F., 1999. Post-Collisional Potassic and Ultrapotassic Magmatism in SW Tibet: geochemical and Sr–Nd–Pb–O Isotopic Constraints for Mantle Source Characteristics and Petrogenesis. Journal of Petrology 40, 1399–1424.
Miller, C., Thöni, M., Frank, W., Schuster, R., Melcher, F., Meisel, T., Zanetti, A., 2003. Geochemistry and tectonomagmatic affinity of the Yungbwa ophiolite, SW Tibet. Lithos 66, 155–172.
Mo, X.X., Hou, Z.Q., Niu, Y.L., Dong, G.C., Qu, X.M., Zhao, Z.D., Yang, Z.M., 2007. Mantle contributions to crustal thickening during continental collision: evidence from cenozoic igneous rocks in southern Tibet. Lithos 96, 225–242.
Mo, X.X., Niu, Y.L., Dong, G.C., Zhao, Z.D., Hou, Z.Q., Su, Z., Ke, S., 2008. Contribution of syncollisional felsic magmatism to continental crust growth: a case study of the Paleogene Linzizong volcanic Succession in southern Tibet. Chemical Geology 250, 49–67.
Mungall, J.E., 2002. Roasting the mantle: slab melting and the genesis of major Au and Au-rich Cu deposits. Geology 30, 915–918.
Najman, Y., 2006. The detrital record of orogenesis: a review of approaches and techniques used in the Himalayan sedimentary basins. Earth-Science Reviews 74, 1–72.
Nomade, S., Renne, P.R., Mo, X.X., Zhao, Z.D., Zhou, S., 2004. Miocene volcanism in the Lhasa block, Tibet: spatial trends and geodynamic implications. Earth and Planetary Science Letters 221, 227–243.
Oyarzun, R., Márquez, A., Lillo, J., López, I., Rivera, S., 2001. Giant versus small porphyry copper deposits of Cenozoic age in northern Chile: adakitic versus normal calc-alkaline magmatism. Mineralium Deposita 36, 794–798.
Patzelt, A., Li, H.M., Wang, J.D., Appel, E., 1996. Palaeomagnetism of Cretaceous to Tertiary sediments from southern Tibet: evidence for the extent of the northern margin of India prior to the collision with Eurasia. Tectonophysics 259, 259–284.
Peacock, S., Rushmer, T., Thompson, A., 1994. Partial melting of subducting oceanic crust. Earth and Planetary Science Letters 121, 227–244.
Peccerillo, A., Taylor, S.R., 1976. Geochemistry of Eocene calc-alkaline volcanic rocks from the Kastamonu area, northern Turkey. Contributions to Mineralogy and Petrology 58, 63–81.
Plank, T., Langmuir, C.H., 1998. The chemical composition of subducting sediment and its consequences for the crust and mantle. Chemical Geology 145, 325–394.
Polat, A., Kerrich, R., 2002. Nd-isotope systematics of ∼2.7 Ga adakites, magnesian andesites, and arc basalts, Superior Province. evidence for shallow crustal recycling at Archean subduction zones. Earth and Planetary Science Letters 202, 345–360.
Qu, X.M., Hou, Z.Q., Zaw, K., Li, Y.G., 2007. Characteristics and genesis of Gangdese porphyry copper deposits in the southern Tibetan Plateau: preliminary geochemical and geochronological results. Ore Geology Reviews 31, 205–223.
Qu, X.M., Hou, Z.Q., Li, Y.G., 2004. Melt components derived from a subducted slab in late orogenic ore-bearing porphyries in the Gangdese copper belt, southern Tibetan plateau. Lithos 74, 131–148.
Rapp, R.P., Watson, E.B., 1995. Dehydration melting of metabasalt at 8–32 kbar: implications for continental growth and crust-mantle recycling. Journal of Petrology 36, 891–931.
Rapp, R.P., Shimizu, N., Norman, M.D., Applegate, G.S., 1999. Reaction between slab-derived melts and peridotite in the mantle wedge: experimental constraints at 3.8 GPa. Chemical Geology 160, 335–356.
Rehkamper, M., Hofmann, A.W., 1997. Recycled ocean crust and sediment in Indian Ocean MORB. Earth and Planetary Science Letters 147, 93–106.
Reich, M., Parada, M.A., Palacios, C., Dietrich, A., Schultz, F., Lehmann, B., 2003. Adakite-like signature of Late Miocene intrusions at the Los Pelambres giant porphyry copper deposit in the Andes of central Chile: metallogenic implications. Mineralium Deposita 38, 876–885.
Richards, J.P., Kerrich, R., 2007. Adakite-like rocks; their diverse origins and questionable role in metallogenesis. Economic Geology 102, 537–576.
Sajona, F.G., Maury, R.C., Bellon, H., Cotten, J., Defant, M., Pubellier, M., 1993. Initiation of subduction and the generation of slab melts in western and eastern Mindanao, Philippines. Geology 21, 1007–1010.
Sajona, F.G., Maury, R.C., 1998. Association of adakites with gold and copper mineralization in the Philippines. Comptes Rendus de l'Académie des Sciences, Series IIA, Earth and Planetary Science 326, 27–34.
Schmitz, M.D., Vervoort, J.D., Bowring, S.A., Patchett, P.J., 2004. Decoupling of the Lu-Hf and Sm-Nd isotope systems during the evolution of granulitic lower crust beneath southern Africa. Geology 32, 405–408.
Sen, C., Dunn, T., 1994. Dehydration melting of a basaltic composition amphibolite at 1.5 and 2.0 GPa: implications for the origin of adakites. Contributions to Mineralogy and Petrology 117, 394–409.
Sha, L.K., Chappell, B.W., 1999. Apatite chemical compostion, determined by electron microprobe and laser-ablation inductively coupled plasma mass spectrometry, as a probe into granite petrogenesis. Geochemica et Commochimica Acta 63, 3861–3881.
Skewes, M.A., Stern, C.R., 1994. Tectonic trigger for the formation of late Miocene Cu-rich breccia pipes in the Andes of central Chile. Geology 22, 551–554.
Söderlund, U., Patchett, P.J., Vervoort, J.D., Isachsen, C.E., 2004. The 176Lu decay constant determined by Lu–Hf and U-Pb isotope systematics of Precambrian mafic intrusions. Earth and Planetary Science Letters 219, 311–324.
Steiger, R.H., Jäger, E., 1977. Subcommission on geochronology: convention on the use of decay constants in geo- and cosmochronology. Earth and Planetary Science Letters 36, 359–362.
Stern, C.R., Kilian, R., 1996. Role of the subducted slab, mantle wedge and continental crust in the generation of adakites from the Andean Austral Volcanic Zone. Contributions to Mineralogy and Petrology 123, 263–281.

Streck, M.J., Leeman, P.W., Chesley, J., 2007. High-magnesian andesite from Mount Shasta: a product of magma mixing and contamination, not a primitive mantle melt. Geology 35, 351–354.
Sun, S.S., McDonough, W.F., 1989. Chemical and isotopic systematics of oceanic basalt: implications for mantle compositions and processes. Geological Society London Special Publications 42, 313–345.
Sun, W.D., Ling, M.X., Yang, X.Y., Fan, W.M., Ding, X., Liang, H.Y., 2010. Ridge subduction and porphyry copper-gold mineralization: an overview. Science China-Earth Sciences 53, 475–484.
Tafti, R., Mortensen, J.K., Lang, J.R., Rebagliati, M., Oliver, J.L., 2009. Jurassic U-Pb and Re-Os ages for the Newly discovered Xietongmen Cu-Au porphyry district, Tibet PRC: implications for metallogenic epochs in the Southern Gangdese Belt. Economic Geology 104 (1), 127–136.
Tang, G.J., Wang, Q., Wyman, D.A., Li, Z.X., Zhao, Z.H., Jia, X.H., Jiang, Z.Q., 2010. Ridge subduction and crustal growth in the Central Asian Orogenic Belt: evidence from Late Carboniferous adakites and high-Mg diorites in the western Junggar region, northern Xinjiang (west China). Chemical Geology 277, 281–300.
Thiéblemont, D., Stein, G., Lescuyer, J.L., 1997. Gisements épithermaux et porphyriques: la connexion adakite. C.R.Acad. Sci. Paris, Sciences de la terre et des planetes/ Earth and Planetary Science 325, 103–109.
Topuz, G., Altherr, R., Schwarz, W.H., Siebel, W., Satır, M., Dokuz, A., 2005. Post-collisional plutonism with adakite-like signatures: the Eocene Saraycık granodiorite (Eastern Pontides, Turkey). Contributions to Mineralogy and Petrology 150, 441–455.
Tu, X.L., Zhang, H., Deng, W.F., Ling, M.X., Liang, H.Y., Liu, Y., Sun, W.D., 2011. Application of RESOlution in-situ laser ablation ICP-MS in trace element analyses. Geochimica 40, 83–98 (In Chinese with English Abstract).
Turner, S., Arnaud, N., Liu, J., Rogers, N., Hawkesworth, C., Harris, N., Kelley, S., Van Calsteren, P., Deng, W., 1996. Post-collision, shoshonitic volcanism on the Tibetan plateau: implications for convective thinning of the lithosphere and the source of ocean island basalts. Journal of Petrology 37, 45–71.
Vervoort, J.D., Jonathan Patchett, P., 1996. Behavior of hafnium and neodymium isotopes in the crust: constraints from Precambrian crustally derived granites. Geochimica et Cosmochimica Acta 60, 3717–3733.
Vervoort, J.D., Jonathan Patchett, P., Blichert-Toft, J., Albarede, F., 1999. Relationships between Lu-Hf and Sm-Nd isotopic systems in the global sedimentary system. Earth and Planetary Science Letters 168, 79–99.
Vervoort, J.D., Plank, T., Prytulak, J., 2011. The Hf–Nd isotopic composition of marine sediments. Geochimica et Cosmochimica Acta 75, 5903–5926.
Wang, B.D., Xu, J.F., Chen, J.L., Zhang, X.G., Wang, L.Q., Xia, B.B., 2010a. Petrogenesis and geochronology of the ore-bearing porpyritic rocks in Tangbula porphyry molybdenum-copper deposit in the eastern segment of the Gangdese metallogenic belt. Acta Petrologica Sinica 26, 1820–1832 (in Chinese with English abstract).
Wang, Q., Wyman, D.A., Xu, J.F., Zhao, Z.H., Jian, P., Xiong, X.L., Bao, Z.W., Li, C.F., Bai, Z.H., 2006a. Petrogenesis of Cretaceous adakitic and shoshonitic igneous rocks in the Luzong area, Anhui Province (eastern China): implications for geodynamics and Cu-Au mineralization. Lithos 89, 424–446.
Wang, Q., Xu, J.F., Jian, P., Bao, Z.W., Zhao, Z.H., Li, C.F., Xiong, X.L., Ma, J.L., 2006b. Petrogenesis of adakitic porphyries in an extensional tectonic setting, Dexing, South China: implications for the Genesis of Porphyry Copper Mineralization. Journal of Petrology 47, 119–144.
Wang, Q., Wyman, D.A., Zhao, Z.H., Xu, J.F., Bai, Z.H., Xiong, X.L., Dai, T.M., Li, C.F., Chu, Z.Y., 2007a. Petrogenesis of Carboniferous adakites and Nb-enriched arc basalts in the Alataw area, northern Tianshan Range (western China): implications for Phanerozoic crustal growth in the Central Asia orogenic belt. Chemical Geology 236, 42–64.
Wang, Q., Wyman, A., Xu, J.F., Jian, P., Zhao, Z.H., Li, C.F., Xu, W., Ma, J.L., He, B., 2007b. Early Cretaceous adakitic granites in the Northern Dabie complex, central China: implications for partial melting and delamination of thickened lower crust. Geochimica et Cosmochimica Acta 71, 2609–2636.
Wang, Q., Wyman, D.A., Xu, J.F., Zhao, Z.H., Jian, P., Zi, F., 2007c. Partial melting of thickened or delaminated lower crust in the middle of eastern China: implications for Cu–Au mineralization. The Journal of Geology 115, 149–161.
Wang, Q., McDermott, F., Xu, J.F., Bellon, H., Zhu, Y.T., 2005. Cenozoic K-rich adakitic volcanic rocks in the Hohxil area, northern Tibet: lower crustal melting in an intracontinental setting. Geology 233, 464–468.
Wang, Q., Wyman, D.A., Xu, J.F., Wan, Y.S., Li, C.F., Zi, F., Jiang, Z.Q., Qiu, H.N., Chu, Z.Y., Zhao, Z.H., Dong, Y.H., 2008a. Triassic Nb-enriched basalts, magnesian andesites, and adakites of the Qiangtang Block (Central Tibet): evidence for metasomatism by slab-derived melts in the mantle wedge. Contributions to Mineralogy and Petrology 155, 473–490.
Wang, Q., Wyman, D.A., Xu, J.F., Dong, Y.H., Vasconcelos, P.M., Pearson, N., Wan, Y.S., Dong, H., Li, C.F., Yu, Y.S., Zhu, T.X., Feng, X.T., Zhang, Q.Y., Zi, F., Chu, Z.Y., 2008b. Eocene melting of subducting continental crust and early uplifting of central Tibet: evidence from central-western Qiangtang high-K calc-alkaline andesites, dacites and rhyolites. Earth and Planetary Science Letters 272, 158–171.
Wang, Q., Wyman, D.A., Li, Z.X., Sun, W.D., Chung, S.L., Vasconcelos, P.M., Zhang, Q.Y., Dong, H., Yu, Y.S., Pearson, N., Qiu, H.N., Zhu, T.X., Feng, X.T., 2010b. Eocene north-south trending dikes in central Tibet: new constraints on the timing of east-west extension with implication for early plateau uplift? Earth and Planetary Science Letter 298, 205–216.
Wang, R., Xia, B., Zhou, G.Q., Zhang, Y.Q., Yang, Z.Q., Li, W.Q., Wei, D.L., Zhong, L.F., Xu, L.F., 2006c. SHRIMP zircon U-Pb dating for gabbro from the Tiding ophiolite in Tibet. Chinese Science Bulletin 51, 1776–1779.
Watson, E.B., Green, T.H., 1991. Apatite/liquid partition coefficients for the rare earth elements and strontium. Earth and Planetary Science Letters 56, 405–421.
Wei, G.J., Liang, X.R., Li, X.H., Liu, Y., 2002. Precise measurement of Sr isotopic compositions of liquid and solid base using (LP) MCICP-MS. Geochimica 31, 295–305 (in Chinese with English abstract).
Wen, D.R., Chung, S.L., Song, B., Iizuka, Y., Yang, H.J., Ji, J.Q., Liu, D.Y., Gallet, S., 2008a. Late Cretaceous Gangdese intrusions of adakitic geochemical characteristics, SE Tibet: petrogenesis and tectonic implications. Lithos 105, 1–11.
Wen, D.R., Liu, D.Y., Chung, S.L., Chu, M.F., Ji, J.Q., Zhang, Q., Song, B., Lee, T.Y., Yeh, M.W., Lo, C.H., 2008b. Zircon SHRIMP U-Pb ages of the Gangdese Batholith and implications for Neotethyan subduction in southern Tibet. Chemical Geology 252, 191–201.
Wiedenbeck, M., Alle, P., Corfu, F., Griffin, W.L., Meier, M., Oberli, F., Quadt, A., Roddick, J.C., Spiegel, W., 1995. Three natural zircon standards for U-Th-Pb, Lu-Hf, trace element and REE analyses. Geostandards and Geoanalytical Research 19, 1–23.
Williams, H., Turner, S., Kelley, S., Harris, N., 2001. Age and composition of dikes in Southern Tibet: new constraints on the timing of east-west extension and its relationship to postcollisional volcanism. Geology 29, 339–342.
Williams, H.M., Turner, S.P., Pearce, J.A., Kelley, S.P., Harris, N.B.W., 2004. Nature of the source regions for post-collisional, potassic magmatism in southern and northern Tibet from geochemical variations and inverse trace element modelling. Journal of Petrology 45, 555–607.
Wu, F.Y., Yang, Y.H., Xie, L.W., Yang, J.H., Xu, P., 2006. Hf isotopic compositions of the standard zircons and baddeleyites used in U-Pb geochronology. Chemical Geology 234, 105–126.
Wu, F.Y., Clift, P.D., Yang, J.H., 2007. Zircon Hf isotopic constraints on the sources of the Indus Molasse, Ladakh Himalaya, India. Tectonics 26, TC2014. http://dx.doi.org/10.1029/2006TC002051.
Xie, L.W., Zhang, Y.B., Zhang, H.H., Sun, J.F., Wu, F.Y., 2008. In situ simultaneous determination of trace elements, U-Pb and Lu-Hf isotopes in zircon and baddeleyite. Chinese Science Bulletin 53, 1565–1573.
Xiong, X.L., Adam, J., Green, T.H., Niu, H.C., Wu, J.H., Cai, Z.Y., 2006. Trace element characteristics of partial melts produced by melting of metabasalts at high pressures: constraints on the formation condition of adakitic melts. Science in China Series D: Earth Sciences 46, 915–925.
Xiong, X.L., 2006. Trace element evidence for the growth of early continental crust by melting of rutile-bearing hydrous eclogite. Geology 34, 945–948.
Xu, J.F., Castillo, P.R., 2004. Geochemical and Nd-Pb isotopic characteristics of the Tethyan asthenosphere: implications for the origin of the Indian Ocean mantle domain. Tectonophysics 393, 9–27.
Xu, J.F., Shinjo, R., Defant, M.J., Wang, Q., Rapp, R.P., 2002. Origin of Mesozoic adakitic intrusive rocks in the Ningzhen area of east China: partial melting of delaminated lower continental crust? Geology 30, 1111–1114.
Xu, W.C., Zhang, H.F., Guo, L., Yuan, H.L., 2009. Miocene high Sr/Y magmatism, south Tibet: product of partial melting of subducted Indian continental crust and its tectonic implication. Lithos 114, 293–306.
Yang, J.H., Wu, F.Y., Chung, S.L., Wilde, S.A., Chu, M.F., 2006. A hybrid origin for the Qianshan A-type granite, northeast China: geochemical and Sr-Nd-Hf isotopic evidence. Lithos 89, 89–106.
Yang, J.H., Wu, F.Y., Wilde, S.A., Xie, L.W., Yang, Y.H., Liu, X.M., 2007. Tracing magma mixing in granite genesis: in situ U-Pb dating and Hf-isotope analysis of zircons. Contributions to Mineralogy and Petrology 153, 177–190.
Yin, A., Harrison, T.M., 2000. Geologic evolution of the Himalaya-Tibetan orogen. Annual Review of Earth and Planetary Sciences 28, 211–280.
Zhang, K.Y., 2005. Study on the prediction of the Ore-finding Target of the Kelu cuproaurite in Zhanang County, Tibet. Geology of Fujian 24, 65–71, in Chinese with English abstract.
Zhang, S.Q., Mahoney, J.J., MO, X.X., Ghazi, A.M., Milani, L., Crawford, A.J., Guo, T.Y., Zhao, Z.D., 2005. Evidence for a Widespread Tethyan Upper Mantle with Indian-Ocean-Type Isotopic Characteristics. Journal of Petrology 46, 829–858.
Zhang, Z.M., Zhao, G.C., Santosh, M., Wang, J.L., Dong, X., Shen, K., 2010. Late Cretaceous charnockite with adakitic affinities from the Gangdese batholith, southeastern Tibet: evidence for Neo-Tethyan mid-ocean ridge subduction? Gondwana Research 17, 615–631.
Zhao, Z.D., Mo, X.X., Dilek, Y., Niu, Y.L., DePaolo, D.J., Robinson, P., Zhu, D.C., Sun, C.G., Dong, G.C., Zhou, S., Luo, Z.H., Hou, Z.Q., 2009. Geochemical and Sr-Nd-Pb-O isotopic compositions of the post-collisional ultrapotassic magmatism in SW Tibet: petrogenesis and implications for India intra-continental subduction beneath southern Tibet. Lithos 113, 190–212.
Zhou, S., Mo, X.X., Dong, G.C., Zhao, Z.D., Qiu, R.Z., Guo, T.Y., Wang, L.L., 2004. ^{40}Ar-^{39}Ar geochronology of Cenozoic Linzizong volcanic rocks from Linzhou Basin, Tibet, China, and their geological implications. Chinese Science Bulletin 49, 1970–1979.
Zhu, D.C., Zhao, Z.D., Pan, G.T., Lee, H.Y., Kang, Z.Q., Liao, Z.L., Wang, L.Q., Li, G.M., Dong, G.C., Liu, B., 2009. Early cretaceous subduction-related adakite-like rocks of the Gangdese Belt, southern Tibet: products of slab melting and subsequent melt–peridotite interaction? Journal of Asian Earth Sciences 34, 298–309.